Proposal for a "Single Tray" Time-of-Flight Patch for STAR.

N. Adams, B. Bonner, G. Eppley, W.J. Llope, G. Mutchler,
E. Platner, P. Yepes
T.W. Bonner Nuclear Laboratory,
Rice University, Houston, TX 77005

M. Kaplan
Carnegie Mellon University,
Pittsburgh, PA 15213

D. Keane
Kent State University,
Kent, Ohio 44242

H.J. Crawford, P.M. Jacobs
Lawrence Berkeley National Laboratory,
Berkeley, CA 94720

C.A. Ogilvie
Massachusetts Institute of Technology,
Cambridge, MA 02139

L. Ray
University of Texas,
Austin, TX 78712

T. Trainor
University of Washington,
Seattle, WA 98185

G.J. Kunde
Yale University,
New Haven, CT 06520

Abstract

We propose the construction of a single "tray" of Time-of-Flight counters and the installation of this tray in STAR in time for operation in the first physics run of RHIC. The design of the system is similar to the present design of the full STAR TOF system, covering -0.07<η<0.95 and $\sim$5.3° in azimuth with 45 single-ended plastic scintillator slats. It will provide velocity information for reconstructed tracks that extends, and nearly completes, the hadronic particle identification capabilities of STAR. High efficiency direct identification of π and K mesons is possible up to $\sim$1.8 GeV/c, while protons can be positively identified up to $\sim$3 GeV/c. The system thus plays a crucial or positive role in a number of fundamental physics analyses in STAR. It also allows important consistency tests of the performance of all of the particle identification approaches used in STAR.

Contents

List of Figures

List of Tables

1 Introduction

The RHIC project is nearing completion, which will open for study an entirely new regime of nuclear and particle physics. The first experiment approved for construction at RHIC is the Solenoidal Tracker at RHIC (STAR). This is a large experiment that was designed to measure the thousands of particles per event at mid-rapidity expected in central Au+Au collisions at 100 GeV/N/beam. STAR has a wide kinematic acceptance and high resolution, allowing it to accurately measure a vast number of different physics observables. Given the lack of unambiguous signatures for the formation of the quark-gluon plasma in RHIC collisions, such a wide-acceptance experiment is crucial. There are, however, certain "blind spots" in the apparatus. The STAR detector cannot directly identify $\sim$40% of the particles leaving tracks in the apparatus. Many basic and important physics analyses are therefore made more difficult or more imprecise. To address this problem, we propose the construction of a small patch of Time-of-Flight (TOF) counters and the insertion of this system into the STAR apparatus in time for the first run of RHIC.

The proposed system is based on the design of the full STAR TOF system,[1] [2] [3] which has been included in STAR since its inception. The full TOF system is a highly-segmented cylinder of small plastic scintillator slats covering the outer surface of the STAR Time Projection Chamber (TPC). The slats are each read-out by mesh dynode photomultiplier tubes. The slat assemblies and electronics chain that follows are optimized for fast timing. The extrapolation of TPC tracks to the TOF system allows the assignment of a time-of-flight for each track. The total track length and the time of flight result in a velocity for each track, which, when compared to the track's momentum, directly measures a mass. If the time differences can be measured to better than $\sim$100 ps, then such analyses allow the direct Particle IDentification (PID) of hadrons with high efficiency to significantly higher momenta than possible from TPC dE/dx alone.

Without TOF information, a gap exists in STAR's hadron PID capabilities between the low momentum particles identified via TPC dE/dx and the high momentum particles identified by the (proposed) Ring Imaging Čerenkov Detector (RICH). The gap obscures a particularly interesting region of hadronic transverse momentum spectra. Near mid-rapidity, it is qualitatively accurate to say that TPC dE/dx identifies primarily late thermal hadrons and pions from resonances, while the RICH identifies hadrons resulting more often from earlier and harder partonic interactions. The present system bridges the important transitional region that includes the onset of mini-jet phenomena. Hadronic PID with TOF information is quite clean for these momenta. The TOF PID is efficient both at low momenta where TPC PID is efficient, and at high momenta where RICH PID is efficient. Thus, important comparisons between the various PID approaches based on the information from TPC, SVT, EMC, and RICH detectors in STAR are possible. This will lead to a more rapid understanding and optimization of *all* of STAR's PID approaches. The RICH, if approved, will exist in STAR for the first three years, while the present system is under no such constraint. The present system is also an important step towards a large-area TOF systems by providing experience on fast timing measurements in STAR which will

be useful even if the full system and the present patch do not have exactly the same design.

The importance of time-of-flight to the physics goals of STAR has been recognized in a number of reviews. The NSAC [4] subcommittee chaired by C.K. Gelbke noted:

> "A small-area TOF array ... will be sufficient to measure inclusive particle ratios and correlate them to other observables measured event-by-event in STAR. Such a smaller array would already significantly enhance the physics capabilities of this experiment. ... STAR should aim at a coverage which is sufficient for event-by-event Kaon (and possibly proton) identification, which in other observables is the prominent feature and strength of STAR. If fiscal constraints are such that this cannot be realized, a small area TOF array would still be very valuable, and further R&D should be encouraged to search for a viable solution for large area coverage."

Such a "smaller array" is the subject of the present proposal. The contributions to STAR's physics program are numerous and are described first. This is followed by the technical description of the proposed system including the results of beam and bench tests. Simulations performed to investigate important aspects of the performance of the system in central Au+Au collisions at RHIC are discussed next. Finally, the costs and schedule for the construction of this system are presented.

2 Contributions to STAR

The primary goal of the proposed TOF system is to provide information that greatly extends the hadronic PID capabilities of the experiment. Such identification with TOF information is clean up to momenta ~1 GeV/c higher than those for which TPC dE/dx PID is efficient. The system thus has important uses for a number of fundamental physics analyses in STAR, as described in section 2.2. The proposed system also allows important studies of the performance of all of the PID algorithms that are used in STAR, as now described.

2.1 Analysis Algorithms

The STAR experiment is composed of a number of sub-detectors that provide information allowing one to identify the species of individual tracks through the detector. The method, the resolution, and the kinematic coverage for the PID capabilities for each detector are different. In this section, the various approaches are described. Throughout the lifetime of the STAR experiment and especially in the first run of RHIC, it will be crucial to have a means of cross-checking the various particle identification approaches to insure consistency in the results. For the majority of the kinematic acceptance of the experiment, such cross-checks are possible only with the availability of TOF information.

2.1.1 Particle Identification via dE/dx

Particle identification (PID) in the STAR TPC and SVT is done using the fact that pions, kaons, and protons are not minimum-ionizing in the energy range of the STAR acceptance and thus exhibit different energy losses while traversing these detectors. Figure 1 shows the expected energy loss curves as measured in the TPC for pions, kaons, and protons.

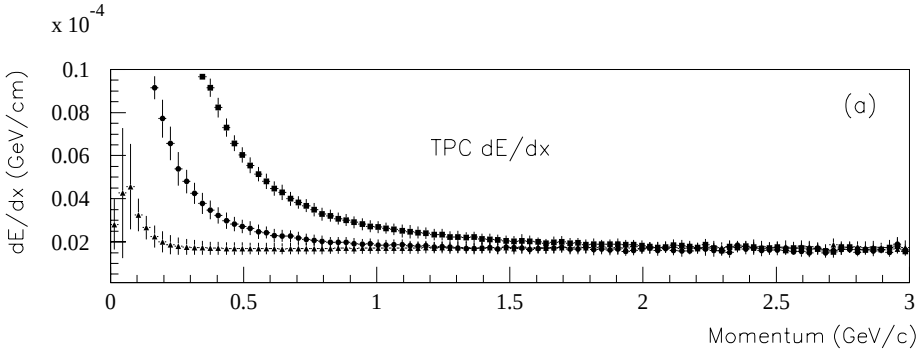

Figure 1: The mean values of the TPC dE/dx for pions, kaons and protons, respectively, versus the track momentum obtained from full STAR simulations. The errors bars are the standard deviations of the dE/dx distributions in each momentum bin.

To perform particle identification with TPC energy loss, functions of the Bethe-Bloch form are fit to these curves. From these fits one can calculate the difference

between the (momentum-dependent) average dE/dx for a particular hadron and the measured energy loss for a given track. With the measured widths of the dE/dx distributions, this difference gives a probability that a given track belongs to a particular hadronic species. At low momenta, where the pion, kaon, and proton separations are large, it is sufficient to make the assignment using the highest probability hypothesis. Above ~350 MeV/c, however, the pion and kaon dE/dx distributions overlap and contamination must be considered. Depending somewhat on the cuts used, hadronic PID with the TPC dE/dx information has the efficiencies and contaminations shown in Figure 2. The efficiency is defined as the total number of correctly tagged particles divided by the total generated in the simulation. The contamination is defined as the number of incorrectly tagged particles divided by the number of correctly tagged particles. It is apparent that proton identification from energy loss in the TPC is efficient only up to momenta of ~1.1 GeV/c, while pion and kaon direct identification is efficient only up to ~0.6 GeV/c.

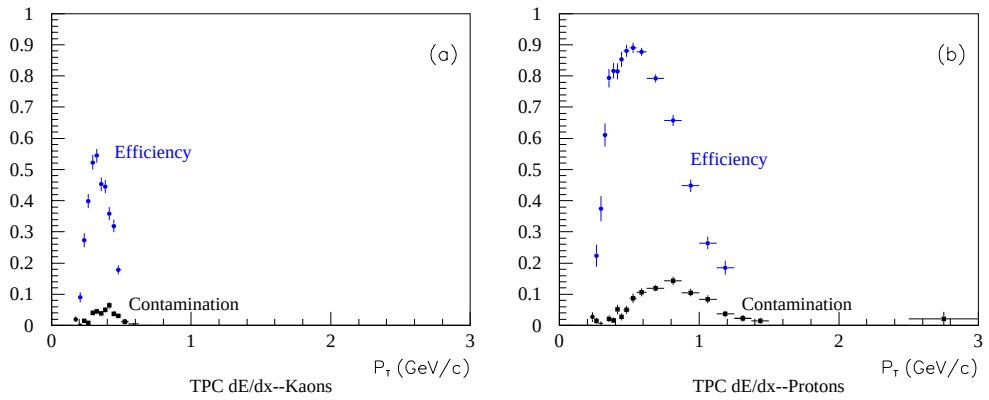

Figure 2: The efficiencies and backgrounds for cuts on the TPC dE/dx bands for the direct identification of K (left frame) and p (right frame) tracks. The error bars are the standard deviations about each mean value.

The TPC can also identify particles if they decay within a fiducial volume of the TPC that allows the reconstruction of both sides of the "kink." Such analyses can identify kaons out to ~3 GeV/c.

Particles also experience energy losses while traversing the Silicon Vertex Tracker (SVT). While the dE/dx resolution in semiconductor detectors such as the SVT is much better than in gas ionization detectors such as the TPC, the SVT provides only three measurements of dE/dx for a typical track as compared to up to 45 from the TPC. The overall resolution on the track dE/dx for PID from the SVT is thus qualitatively similar to that from the TPC. According to the left frame of Figure 3, π/K(K/p) identification using SVT dE/dx is possible up to cut-off momenta of ~0.5(0.8) GeV/c. Not shown in this frame is momenta higher than 0.8 GeV/c, for which direct π/K/p identification is no longer possible. As there is no relativistic rise in particle energy losses in solids, there is a region at these higher momenta where electron identification is again possible [5]. An example is shown in the right frame of Figure 3.

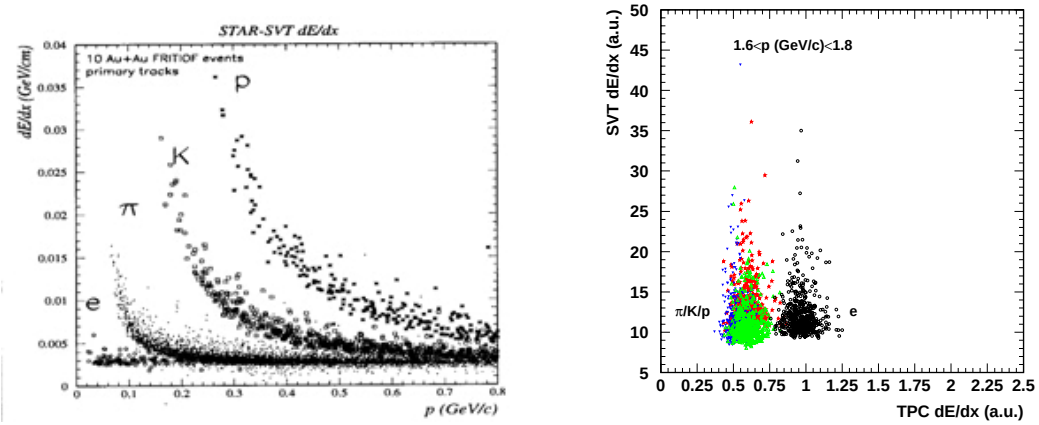

Figure 3: The dE/dx bands for energy loss in the SVT for momenta below 0.8 GeV/c (left frame), and the correlation of the SVT dE/dx versus the TPC dE/dx in a higher momentum bin (right frame), both obtained from full STAR simulations.

2.1.2 Particle Identification via Calorimetry

STAR is also to be equipped with a Pb/scintillator sampling ElectroMagnetic Calorimeter (EMC), which is capable of electron/hadron discrimination on the basis of a number of observables. An electron to hadron discrimination on the order of 80-100:1 is expected for momenta above ∼2 GeV/c. The calorimeter is unable to distinguish pions, kaons, and protons at any momenta, with one exception. The measurement of annihilation energies in the EMC can be used to identify antiproton tracks, but this approach is restricted to very low momenta and is only possible if the EMC tower occupancies are also low. The EMC is capable of reconstructing π^0 mesons using the information from a finely segmented Shower Maximum Detector that is embedded inside the EMC stack.

2.1.3 Particle Identification in RICH Detectors

A RICH detector has recently been proposed [6] to be added to STAR for the first run of RHIC. This detector exploits the fact the Čerenkov light opening angle differs for pions, kaons, and protons at specific momenta. By following TPC tracks to the RICH, one can test various track mass hypotheses by counting the number of lit pixels of the detector within the Čerenkov cone appropriate for the track's identity, its momentum, and its position and angle of incidence in the RICH. Different mass particles produce rings of Čerenkov photons of different radii, as shown in Figure 4. Non-normal tracks simply skew Čerenkov circles into Čerenkov ellipses.

According to Ref. [6], direct identification of pions is possible in the range ∼0.7 to ∼3 GeV/c, kaons from ∼1.1 to ∼3 GeV/c, and protons from ∼1.5 to ∼5 GeV/c. The (kaon)proton identification probability rises with increasing momentum, and reaches 30% at ∼1.1(2.0) GeV/c. The pion PID capability just reaches low enough in momentum to have some overlap with the PID based on the TPC dE/dx. For K and p identification, however, there are gaps of ∼0.5-1 GeV/c between efficient TPC PID and efficient RICH PID. Thus, the comparison of the PID information from

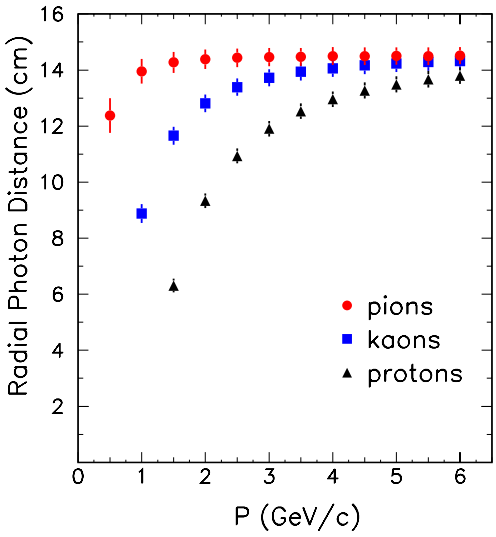

Figure 4: GEANT simulation results for the mean radial distance of photons as detected by the RICH relative to the location of the minimum ionizing particle plotted as a function of the transverse momentum of the charged particle. The error bars are the standard deviations about each mean value.

the TPC and RICH detectors is possible only for pions and only in a very narrow range of momenta near 0.6 GeV/c. This greatly limits one's ability to use TPC PID information for understanding the RICH PID performance, and vice versa.

2.1.4 Particle Identification via Time-of-Flight

In this approach, the absolute time interval between the occurrence of an event and the arrival of a particle at a specific location is measured. Tracking information from the TPC provides the momentum of a particle, and the total path length from the collision vertex to the measurement location. The total path length so measured by the TPC and the time-of-flight lead to a velocity, β, for each track, which, when compared to the track momentum, predicts a mass for each track. Shown in Figure 5 is the measured values of $1/\beta$ vs. the momentum for pions, kaons, and protons obtained from full STAR simulations. The time-of-flight counters tile the TPC outer field cage at the same radius of the CTB, which is $\sim$2.2 m from the beam pipe. The times of flight used to calculate the velocities in this figure are corrected for propagation time of the scintillation light in the slat (*cf.* section 4.2 below).

The resolution of the slat assemblies used in this simulation was that measured for 1.5 cm thick BC408 scintillators in a test beam [20], *i.e.* 60 ps for near-end hits and 100 ps for far-end hits, which implies a geometrically averaged slat resolution of 77 ps. We note that this performance of the slat assemblies, and hence the PID performance, is improved in the present system as discussed in section 3.2.1 below. For central HIJING events, the momentum cutoff predicted by the full simulations, with a 77 ps average slat resolution and the hit position correction, for 2σ π/K separation is 1.8 GeV/c, while K/p separation at the 2σ level exists up to momenta near 3 GeV/c. The large separation in the times of flight for the different particle species allows one

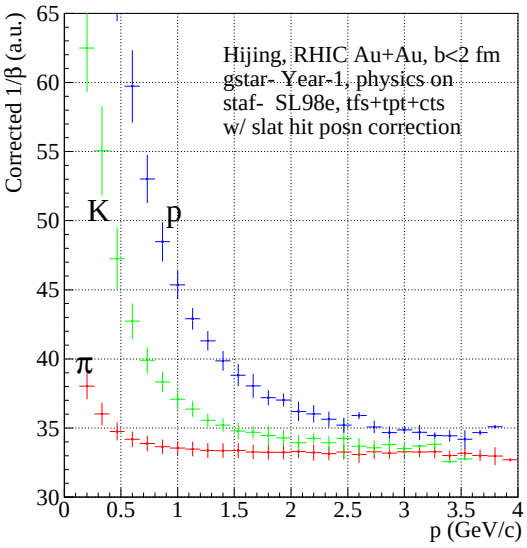

Figure 5: The mean values of the track inverse velocity corrected for the position of the hit along the struck slat as a function of the track momentum. The error bars are one standard deviation of the time of flight distributions at the measured momenta. The position-averaged slat assembly resolution in this simulation was 77 ps.

to cleanly identify particles out to much higher momenta than possible when using dE/dx information alone (*cf.* Figure 1). The TOF system extends the momentum range over which direct hadronic PID is possible by over 1 GeV/c.

2.1.5 Cross-checks

According to the discussion above, the availability of TOF information fills important holes in the acceptance of the experiment. It provides direct PID capabilities in momentum regions where dE/dx-based analyses are no longer efficient. It is also important to notice that crucial cross-checks of the information from various particle identifying detectors in STAR is possible only with the availability of TOF information.

Table 1: A comparison of the approximate momentum regions, in GeV/c, within which direct PID of π, K, and p hadrons is efficient in the different STAR detectors.

	π	K	p
TPC dE/dx	$0.15 < P < 0.6$	$0.15 < P < 0.6$	$0.15 < P < 1.1$
TPC kinks		$P \lesssim 3$	
SVT dE/dx	$0.15 < P < 0.5$	$0.15 < P < 0.5$	$0.15 < P < 0.8$
RICH Č	$0.6 < P < 3$	$1.1 < P < 3$	$1.5 < P < 5$

Shown in Table 1 is the approximate momentum regions for which individual STAR detectors can provide information allowing efficient direct hadron identification. The dE/dx information from the TPC and the SVT is useful for PID at relatively

low momenta. TOF-based PID is also highly efficient here, allowing important tests of the algorithms used to extract PID information from dE/dx measurements. As a limited number of samples of the track dE/dx are available from the tracking detectors, the resolution with which these detectors measure an average dE/dx for each track depends strongly on the number of clusters assigned to each track, the angles the track makes with respect to the detector drift directions, and other factors such as the actual noise level during a run relative to the detector gain. The correlation of the PID information from the TOF versus that from these tracking detectors will allow one to optimize the PID algorithms applied to the TPC and SVT data.

Similar arguments can be made for the extraction of PID information for hadrons from the (proposed) RICH. Except for pions with momenta very close to $\sim$0.6 GeV/c, only the TOF information overlaps kinematically with the information from the RICH. The need for TOF information to understand the information from the RICH was noted explicitly [6] in the RICH proposal.

With a TOF system in place, the performance of the various dE/dx-based PID analyses can be *measured experimentally* for each track that strikes a TOF slat. This allows one to test whether the efficiencies and backgrounds one extracts for a particular PID approach from embedding simulations is in accord with that measured by using the TOF information to select "pure" samples of particular hadrons. Likewise, at higher momenta the efficiencies and backgrounds for the RICH PID will be experimentally measurable by studying tracks striking the RICH in samples purified via TOF analyses. The converses are also true. The TPC, SVT, and RICH PID information can, in specific momentum regions, be used to understand the performance of the TOF system, and of the software that provides the tracking information needed by TOF analyses.

The ability to cross-check of the various PID algorithms will be important throughout the lifetime of STAR, but it is especially so during the commissioning of STAR during the first run of RHIC. STAR will more rapidly converge on the correct software, the correct cuts, and the correct efficiencies and backgrounds for all PID approaches given the availability of TOF information.

2.2 Physics Capabilities

The proposed TOF patch for STAR will make precise high-quality measurements of the spectra and yields of π, K, p, and fragment emission in classes of events selected based on global event observables and/or event-by-event observables. The analyses enabled or enhanced with the availability of TOF information are fundamental and numerous. The main physics goals in Au+Au collisions are described in this section. The use of the present system in STAR's peripheral physics program has not yet been simulated, although comments on the performance of the present system in very peripheral collisions are made in section 4.4.

2.2.1 Net Protons

The collision of the incoming nucleons results in the transport of net baryon number away from the beam rapidity. The energy lost during these collisions will appear in the final state in other degrees of freedom, including nucleon excitations. The degree to which the incoming energy is transfered into the reaction zone is refered to as *energy stopping*; the transfer of net baryon number away from beam rapidity is refered to as *baryon stopping*. The transfer of energy and net baryon number into the reaction zone sets the initial conditions of the reaction, and their experimental determination is crucial to understanding the further evolution of the collision. As examples, a finite net baryon density (*i.e.* an imbalance in the density of light quarks and antiquarks) will result in strangeness enhancement in the QGP phase, and due to the large meson-baryon cross sections, it will profoundly alter the properties of the high density hadronic phase relative to baryon-free matter. Energy and baryon stopping are closely related only near beam rapidity, where a nucleon still carries a large fraction of its incident energy. At midrapidity, the net baryon number is a very weak constraint on the overall distribution of energy in the reaction zone.

Baryon stopping is most commonly measured through the rapidity distributions of net protons (the difference between proton and antiproton distributions), and is usually considered as a low P_T, multiple scattering process. On the other hand, the ratio antiproton/proton at high P_T has been proposed as a means to distinguish the fragmentation of gluon and quark jets and thereby to study the relative energy loss of high P_T gluons and quarks propogating through dense matter. The distinction to be drawn here is between multiple soft collisions and a single large momentum transfer process, both bringing valence quarks from the beam to midrapidity, but possibly at different regions of P_T. It is essential to map out the interference between these processes, and the P_T region in which only TOF can identify protons (lying between the upper boundary in P_T for dE/dx in the TPC and the lower boundary of the RICH) is critical in this regard.

The proposed TOF patch will measure the rapidity distributions, dN/dy, of protons and antiprotons over roughly a full unit of pseudorapidity in the range $\sim 0.06 < \eta < 0.95$. For protons, direct PID from the TPC dE/dx is efficient up to ~1.1 GeV/c. At a pseudorapidity of η=0.95, this implies proton rapidity spectra are measured out to y=0.64 via the dE/dx PID. The TOF identifies protons efficiently up to ~3 GeV/c, which allows the measurement of rapidity spectra out to y=0.88.

The dN/dy spectra for the different hadrons must be corrected for the momentum dependent efficiency for the direct identification of each hadron. One in effect extrapolates the transverse momentum spectra into the regions for which the PID algorithms are inefficient. The uncertainties of such extrapolations are reduced dramatically if TOF information is available. It will be shown in section 2.2.6 below that 50-60% of the protons in central Au+Au events can be directly identified in STAR using only the TPC dE/dx, while more that 95% of the protons in the acceptance of the TOF system are identified directly via time of flight. Thus, useful dN/dy spectra for protons involve transverse momentum acceptance corrections that are a factor of ~2 smaller given TOF information. If a correction factor is decreased, the uncertainty

in the correction is necessarily decreased as well.

The RICH covers a smaller range in pseudorapidity, and the Forward TPC has no PID capabilities. Thus, the proposed system is the only detector in STAR that (with the tracking information from the TPC) makes a net-proton measurement with high PID efficiencies and small corrections over ∼1 unit in rapidity.

2.2.2 Expansion & Thermalization

Transverse momentum distributions provide important information on the reaction dynamics and the temperature reached in the dense matter produced in heavy-ion collisions. They are an avenue towards the measurement of the contributions of collective versus thermal processes. The classical signature of radial flow is an increase in the mean transverse momentum with the particle mass. If thermal equilibrium is achieved, then the spectra for different hadrons are predictable and depend only on the temperature and the radial flow velocity. Deviations from this behavior indicate the importance of non-equilibrium effects produced perhaps by, *e.g.*, regions of QGP within the excited hadronic system.

Shown in Figure 6 are the transverse momentum spectra for pions, kaons, and protons from the codes HIJING [7], RQMD [8], and VENUS [9] for central ^{197}Au+^{197}Au collisions at 100 GeV/N/beam. These distributions cannot be described by a single slope, so a measurement of these over the limited range allowed with the PID capabilities of the TPC dE/dx alone is not sufficient.

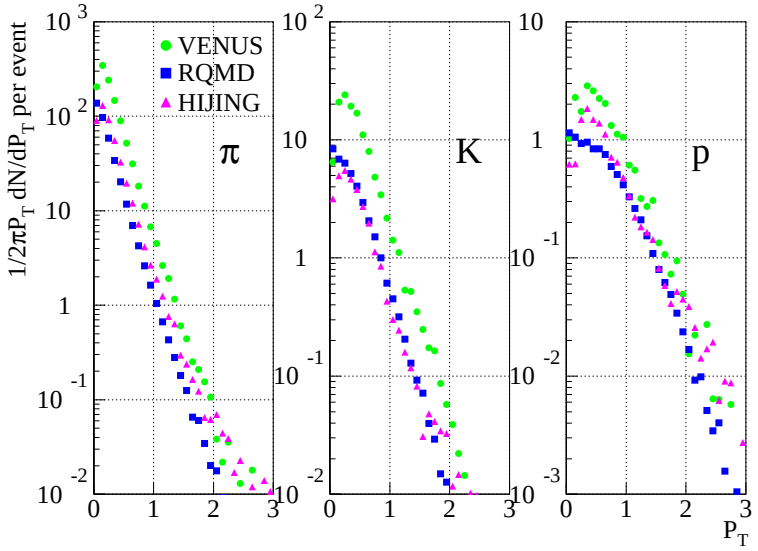

Figure 6: The transverse momentum distributions for pions, kaons, and protons with $|y|<1$ for central collisions from the models HIJING, RQMD, and VENUS.

It has been suggested [13] that the measurement of the mean transverse momentum of particular hadrons and plotting this quantity versus the hadron's mass allows one to evaluate the contribution of hydrodynamical processes. Shown in Figure 7 is the prediction for this effect.

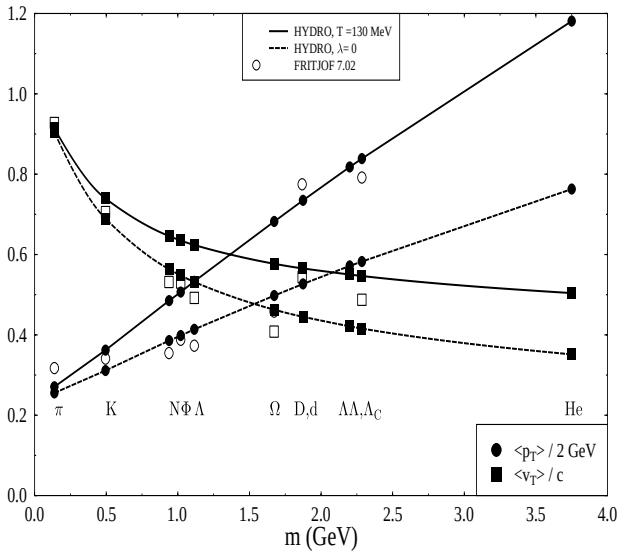

Figure 7: The average transverse momentum and velocity of direct thermal hadrons on the boundry between the mixed phase and pure hadronic phase, λ=0, and on the T=130 MeV isotherm, for central Au+Au collisions at RHIC (from Ref. [13]).

This measurement requires the ability to distinguish the various hadrons up to momenta sufficiently in excess of their individual mean transverse momenta so that an accurate average value can be formed. Using the distributions shown in Figure 6 as a guide, this implies direct hadron PID is needed to at least $\sim$2$\times$400 MeV/c for pions, $\sim$2$\times$600 MeV/c for kaons, and $\sim$2$\times$800 MeV/c for protons, or, to at least 0.8, 1.2, 1.6 GeV/c for π, K, and p, respectively. PID algorithms based on the TPC dE/dx alone cannot approach these momenta.

The experimental test of Figure 7 in STAR also requires the measurement of fragments as well. If one looks only at pions, kaons, and protons, the non-linearities in the $\langle P_T \rangle$ versus the mass may be small relative to the systematic effects, at least early on. Any model - hydrodynamic, soft (Schwinger-like) string fragmentation, and even $g+g \rightarrow q+\bar{q}$ processes, tends [15] to an increase of $\langle P_T \rangle$ with the quark/hadron mass, which, to some level, will always appear "linear" if it is only viewed for π, K, and p tracks. A more convincing physics case is made by extending the $\langle P_T \rangle$ measurement to higher masses by including the values measured for the deuteron and other nuclear fragments. As described in section 3.6 below, the dynamic range of the time difference measurement is at least a factor of five, which implies all of the deuterons with momenta above $\sim$400 MeV/c do not result in TOF TDC overflows. According to RQMD 2.4 [16], more than 90% of the deuterons produced in central Au+Au collisions at 100 GeV/N/beam have momenta above $\sim$0.4 GeV/c. Incidentally, this momentum lower limit of the acceptance of the TOF system for deuterons is the same as that for the identification of deuterons via the TPC dE/dx due to overflows in the 10 bit-equivalent ADCs used to measure the dE/dx. The TOF system thus identifies deuterons over a momentum region very similar to that for which deuteron PID via TPC dE/dx is possible. This will strengthen the measurement of nuclear fragments in STAR and hence improve, among other things, the measurement of $\langle P_T \rangle$ versus

the mass by essentially doubling the mass region under study.

2.2.3 Strangeness

The ratios K/π and K^+/K^- either as a function of temperature or the baryon chemical potential has been suggested as signatures of the QGP [14]. However, the amount of strangeness can be changed during the late hadronic phase of the reaction. Hadrons collide and excite resonances, which can collide further and produce strange particles. Disentangling this mechanism from a QGP-based strangeness enhancement requires the systematic study of different entrance channels including p+A and peripheral A+A reactions.

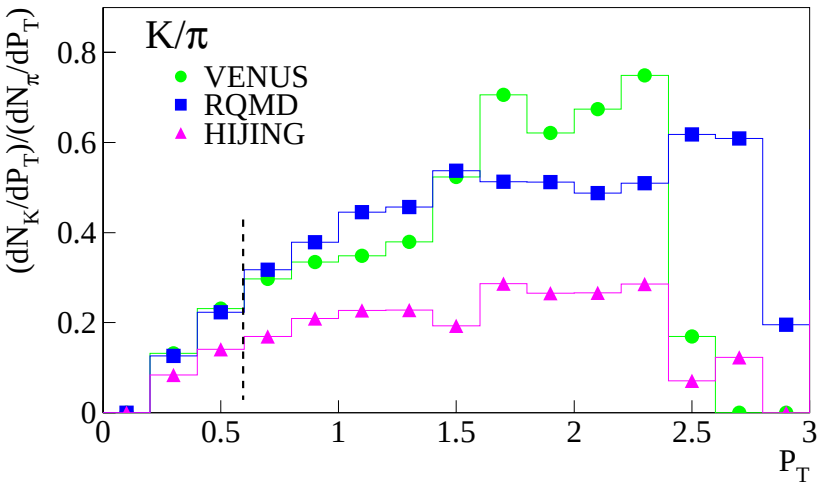

Figure 8: The kaon/pion ratio of P_T spectra measured in the rapidity range $|\eta|<1$. The region in transverse momenta for which there is direct PID from TPC dE/dx alone for these two particles is to the left of the dashed vertical line.

The ratio of K and π cross sections is plotted as a function of P_T in Figure 8 for central events from the HIJING, RQMD, and VENUS models. The TPC dE/dx directly identifies these particles only for transverse momenta to the left of the dashed line. While the ratios from VENUS and RQMD differ significantly from that from HIJING below ~0.6 GeV/c, it is not until these ratios are viewed out to at least 1.5 GeV/c that the three models differ significantly. To fully characterize the momentum dependence of these ratios thus requires TOF information. The study of these ratios in different Au+Au event classes in STAR, as well as in p+p and p+A reactions, then allows searches for the onset of enhancements in strangeness production.

2.2.4 Interferometry

Two-particle correlations probe the space-time dynamics of particle emission from heavy-ion collisions. The original goal of the technique was to extract information on the geometrical size of the emitting source via the quantum interference of identical particles, *i.e.* HBT analyses of intensity interferometric correlation functions.

However, the dynamics of the reaction causes additional correlations between particles, making the extraction of geometrical information from momentum correlations difficult. Recently, this complicating dependence on the dynamics has been turned around. Now, two-particle correlations are also used to probe the dynamics of the reaction. In particular, the dependence of the interferometric parameters as a function of the transverse momentum and rapidity of the pair provides information on the expansion of the system. This information can be combined with single particle spectra and coalescence analyses of fragment production to provide stringent constraints on the amount and type of collective flow.

To study hadron flow in STAR via the momentum dependence of interferometric parameters over a wide range of pair momenta requires the extended PID capabilities provided by the TOF system. The extension of the pair momentum region with direct PID also leads to smaller extrapolations to estimates of the pion phase space density [17]. This quantity is of interest for the study of multi-pion Bose-Einstein effects, and for an accurate prediction of the di-lepton spectra from $\pi^+ + \pi^-$ annihilation.

These studies can of course be performed in any number of event classes. For example, in those events with a mean transverse momentum above the ensemble average, interferometry can be used to investigate the amount of flow. This illustrates how interferometry with the extended PID provided by the TOF patch can be combined with the event-by-event capabilities to make detailed assessments of the physics at work in STAR event classes.

In principle, the TOF patch allows interferometric analyses of $\pi\pi$ and KK pairs up to $\sim$1.8 GeV/c, and pp pairs up to $\sim$3.0 GeV/c. It should be noted that the tracking resolution reduces these upper limits somewhat. If a typical radius parameter is 10 fm, the momentum resolution needed to resolve relative momenta well enough to see the correlations is $\hbar c/10$ fm, or 20 MeV. Assuming the TPC resolution at mid-rapidity is ΔP/P=1.5%, then at (1.8)3 GeV/c the momentum resolution on each track is 27(45) MeV/c, which is comparable or larger than the $20\sqrt{2}$=28 MeV/c scale of interest. The TPC tracking resolution this limits correlation analyses to individual track momenta of up to $\sim$1.5 GeV/c or so. For $\pi\pi$ and KK correlations, this is still a factor of 2.5 above that possible with dE/dx PID alone. The rates for pairs of identified particles at low relative momentum but large total momentum may be too low to allow interferometry in three or more dimensions in RHIC's first year, although the simulations needed to make estimates for the pair rates with TOF PID have not been performed.

2.2.5 High P_T

A sensitive probe of the QGP is one that both reflects some property of the early partonic stage of the reaction and retains this information during the intense hadronic scattering in the late hadronic phase. One observable that satisfies these requirements is the yield of particles at high transverse momenta. Partons at high momenta leave the collision zone before the plasma hadronizes and are causally disconnected from the hadronic exit stage and hence retain any information they have on the QGP. As high momentum partons ($>$ 2 GeV/c) travel through the plasma, they are predicted

to lose energy at the rate of approximately 1 GeV/fm. The rate of energy loss is sensitive to the nature of the reaction, *i.e.* whether more energy is distributed in quasi-free quarks rather than in quarks correlated in hadrons. The slowed-down partons fragment into hadrons, therefore any energy-loss in the plasma will soften the measured hadronic spectra, which reduces the measured rates at high P_T. The present system significantly widens the momentum range over which hadrons can be identified directly. The particle identification capabilities provided by the TOF system extend well into the "transition" regions of transverse momentum spectra that indicate the onset of semi-hard to hard partonic interactions.

The suppression of diquarks has also been proposed [11] as a signature of QGP formation in heavy-ion collisions. This would be detectable as a suppression of high P_T nucleons. The detection of mini-jets through the accurate measurement of P_T tails has been also proposed [12] as a signature for QGP. The suppression of mini-jets will be manifested in a diminution of high P_T particles. In this case the suppression should be present for all particle species. To accomplish these goals, the different particle species obviously must be studied separately over wide momentum ranges.

The discrimination between π and K at 2σ occurs up to $\sim$1.8 GeV/c. However, for all momenta the kaons are less abundant than pions. Subtracting the kaon contamination from the identified pions should thus be a tractable analysis problem at these momenta. This will enable charged pion spectra to be measured over the semi-hard to hard momenta from near zero to near $\sim$3 GeV/c, where the proton band then begins to intersect the π-K band. Given samples large enough to support it, this could be pushed farther still. At some level it will be possible to correct for the proton contamination in the π-K band, perhaps pushing the ability to measure pion transverse momentum spectra above 3 GeV/c. This capability complements the recently proposed RICH detector in that the TOF and RICH overlap kinematically for $\eta \lesssim 0.3$, while the TOF extends the rapidity range for such analyses out to $\eta \sim 0.95$. The TOF system will continue to contribute to STAR's high-P_T physics program after the RICH detector is returned to CERN after RHIC's third year.

2.2.6 Experimental Acceptance

During the first run of RHIC, the central detectors in STAR's data stream will be the full TPC, the full barrel of CTB, and a small patch of EMC. Efficient hadron PID is possible via dE/dx in the TPC, and some electron and photon PID will be available from the EMC patch. The second year of RHIC running will see the availability of the SVT, and an approximate doubling of the number of installed EMC modules. While the SVT greatly improves the tracking performance of the experiment and, in some kinematic regions, its ability to identify electrons, it does not appreciably improve the efficiency or the kinematic coverage of π/K/p PID.

It is therefore not unfair to say that the funded detector systems in STAR in the first years of running can positively identify with high efficiency only those pions with momenta below $\sim$0.6 GeV/c, and only those protons with momenta below $\sim$1.1 GeV/c. While avenues towards the kaon content in the reactions exist in the reconstruction of Kaon kinks, and via Ks$\rightarrow\pi^+\pi^-$ reconstruction, the additional direct

identification of Kaons via their time-of-flight will be important to understand the Kaon results obtained from these very different approaches. While the acceptance of STAR's tracking detectors is on the order of ~95% within ~3 units of pseudorapidity of the central region, the acceptance considering STAR's ability to positively identify the mass of each track is significantly smaller. For all but the simplest physics analyses, it is the experiment's acceptance for directly identified tracks that really matters.

Shown in Table 2 are multiplicities per event of pions, kaons, and protons in various total momentum regions obtained from HIJING, VENUS, and RQMD for central ^{197}Au+^{197}Au collisions. The multiplicities shown in the columns labelled "dE/dx" and "TOF" have the following meaning. For the former, these are the multiplicities of pions and kaons with momenta below 0.6 GeV/c and protons with momenta below 1.1 GeV/c. For the latter, these are the multiplicities of pions and kaons with momenta below 1.7 GeV/c and protons with momenta below 2.8 GeV/c. These momentum regions correspond to those for which direct PID is efficient from the TPC dE/dx, and from the TOF, respectively.

Table 2: The multiplicities of various hadrons with rapidity $|\eta|<1$ and all azimuthal angles obtained from central HIJING, VENUS, and RQMD events in specific momentum regions. The multiplicities themselves are shown in the upper four rows, while they are expressed as percentages of the appropriate totals in the lower four rows. The momentum regions chosen are described in the text.

	HIJING			VENUS			RQMD		
	tot.	dE/dx	TOF	tot.	dE/dx	TOF	tot.	dE/dx	TOF
$\pi^{\pm}$	1248	786	1227	3387	2126	3358	976	620	964
$K^{\pm}$	132	46	127	590	207	573	171	48	164
$p^{\pm}$	75	48	73	138	84	136	48	23	46
sum	1455	880	1427	4115	2417	4067	1195	691	1174
$\pi^{\pm}$	1248	63%	98%	3387	63%	99%	976	64%	99%
$K^{\pm}$	132	35%	96%	590	35%	97%	171	28%	96%
$p^{\pm}$	75	64%	97%	138	61%	98%	48	48%	96%
sum	1455	60%	98%	4115	59%	99%	1195	58%	98%

According to this table, the overall acceptance for the experiment with direct PID in the region $|\eta|<1$ is only on the order of ~60%, which is poor considering that the geometrical acceptance and tracking efficiencies in this region are on the order of ~95%. Due to the fact that the mean transverse momenta of kaons is ~50% larger than that for pions, the acceptance for identified kaons is smaller still. Only about a third of the kaons produced in the HIJING and VENUS events can be directly identified using energy loss in the TPC. The availability of TOF information increases the acceptance significantly, bringing it above 95% for all three hadrons.

The present proposal is of course not for a system that covers the full azimuth. However, this is simply a question of collecting more events and applying the geomet-

rical acceptance of the present patch compared to the full surface of the TPC. Such a correction is trivial. The event sample sizes needed to attack the physics goals of the present system are quite modest. In Ref. [18], for a 12 tray (10%) patch of TOF it was estimated that ∼50k events per sample would be necessary to study the physics described above with a sufficient statistical certainty. This corresponds to ∼14 hours of STAR running at 1 Hz. Statistically equivalent spectra are thus obtained with the present single tray after about one week of running at 1 Hz (∼0.6 M events), *i.e.* after a few weeks of real time. At this point, the limited geometrical acceptance of the TOF patch compared to the total area of the TPC cylinder is no longer an issue, except for event-by-event physics (see below).

The proposed TOF system thus *effectively* increases the acceptance of the experiment by very significant amounts. Considering the very modest cost of the present system compared to the cost of STAR, the impact that the proposed system would have on the physics reach the experiment is dramatic.

Obviously, this argument applies to the study of particular samples of events, not to *the formation* of such samples based on event-by-event (EbyE) criteria based on TOF information. The patch proposed here has too limited of a geometrical acceptance in single events to make significant contributions to the measurement of EbyE observables [2], *e.g.* the number of TOF-identified Kaons in single events or the TOF-identified K/π ratio in single events. However, this should not be taken to imply the present system cannot contribute to STAR's EbyE physics program. Indeed, one can easy imagine the formation of specific samples of events based on a number of other EbyE observables, such as the apparent temperature, total number of charged particles, charged to neutral ratio, and so on. If such samples are sufficiently large, the present system can expose aspects of the events in each sample that not accessible to the baseline detectors, such as identified particle mean transverse momenta, spectral shapes, and so on.

3 Technical Description and Test Results

3.1 Introduction

A mature design for the full STAR TOF system has existed for years. This design is based on a number of test beam and bench measurements that have been published in journals and as STAR notes. Members of the present group have built and successfully operated time-of-flight systems in other experiments. This experience and previous R&D work guides the technical aspects of the present proposal, which are described in this section. To achieve the physics and analysis goals, the TOF system must measure the flight times of charged tracks in the central region of STAR with an overall resolution of better than 100 picoseconds.

A quarter section of the STAR detector is shown in Figure 9. The envelope for the Central Trigger Barrel (CTB) is immediately outside of the TPC. The straight-line distance from the interaction vertex to the CTB envelope ranges from $\sim$2.2 m at pseudorapidity η=0 to $\sim$2.9 m at η=1. The CTB, which is technologically similar to the presently proposed TOF system, consists of a total of 240 long scintillator slats housed in 120 "trays" which cover in total $|\eta|<1$ and 2π in azimuth.

We propose here the replacement of one of these CTB trays with a tray containing similar detectors but optimized for time of flight measurements. The design of this tray of TOF is based on the design of the full STAR TOF system. The full system is a highly segmented cylinder of 2.2 m in radius and 4.3 m in length. It covers the outer radius of the STAR TPC with 6000 single-ended plastic scintillator slats arranged in 120 trays of 50 scintillators each. A tray subtends one unit in pseudorapidity and 6° in azimuth, and, in each tray, there are five rows of slats in azimuth, and ten rows of slats per unit psuedorapidity.

The smaller scope of the present proposal and specific constraints, described below, imply that certain deviations from the existing design of the full STAR TOF system are sensible. In all aspects of the design of the present system, the most proven and conventional of the options available were the ones chosen. This will minimize the time and effort to implement the system.

The components of the system are as follows. The slat assemblies include the plastic scintillator slats, the transducer that converts the scintillation light into an electrical signal, and the wrapping that light-tights the scintillator and optimizes the magnitude and shape of the signal. The electronics that power the transducer are discussed as part of the slat assemblies. Simple electronics boards are included "on-board" for a specific conversion of the signals, discussed below, that is needed to achieve the fast timing performance in the presence of long signal cables. The active elements and the electronics are housed in the same type tray used for the CTB, which provides the mechanical support for the TOF slat assemblies, the on-board electronics, and water cooling loops that remove heat from the interior of the tray. Unlike the full STAR TOF system, the signals from the present system are digitized outside of the trays, after several hundred feet feet of cable on the STAR electronics platforms. Each of the components of the present system is now discussed in turn.

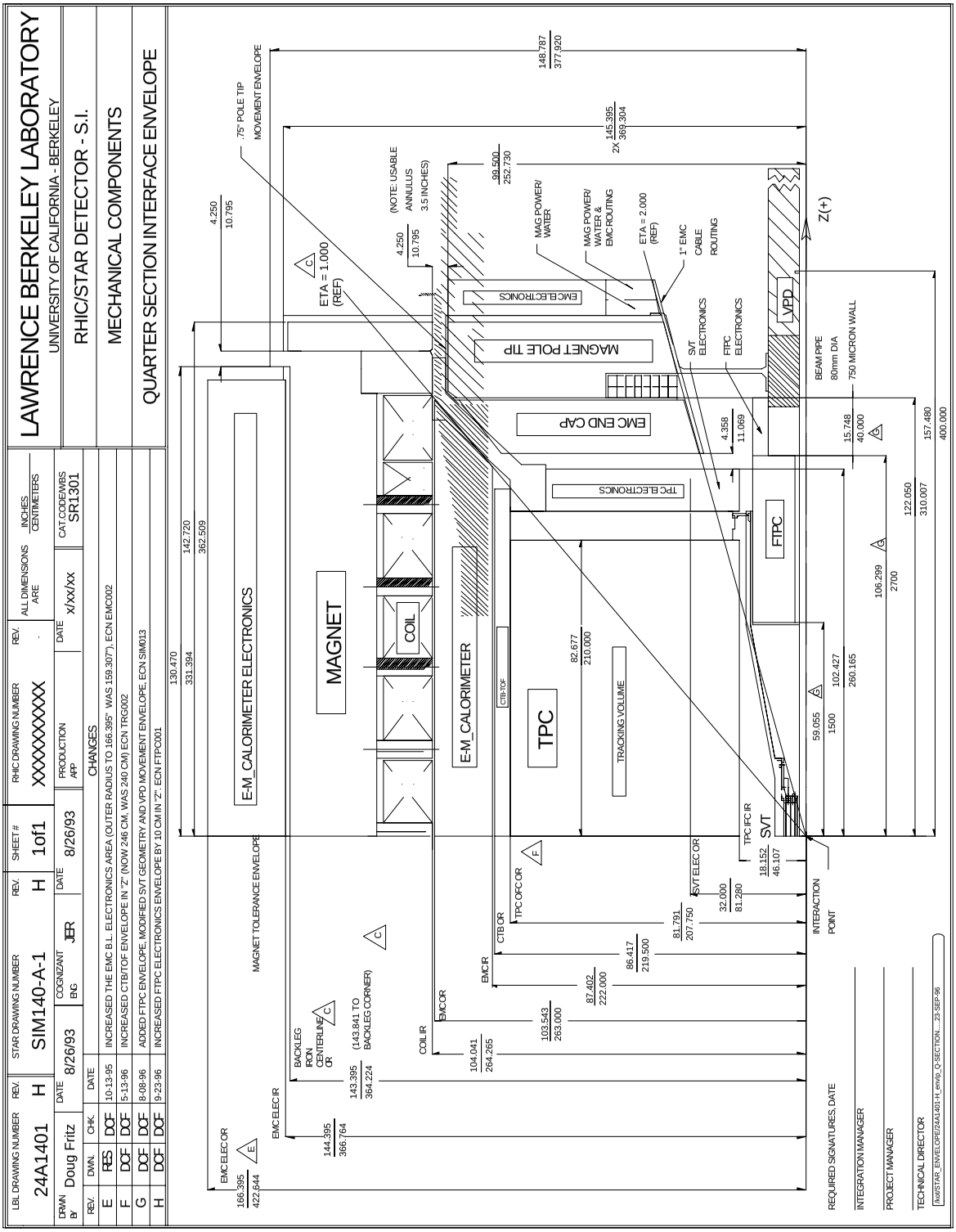

Figure 9: A quarter-section of STAR indicating the various detector envelopes.

3.2 Slat Assemblies

The active elements of the present TOF system are the slat assemblies, each of which consists of a plastic scintillator, an optical transducer, and existing electronics to power the transducer. These components, and the particular choices made for each to optimize the performance of the system, are described in this subsection.

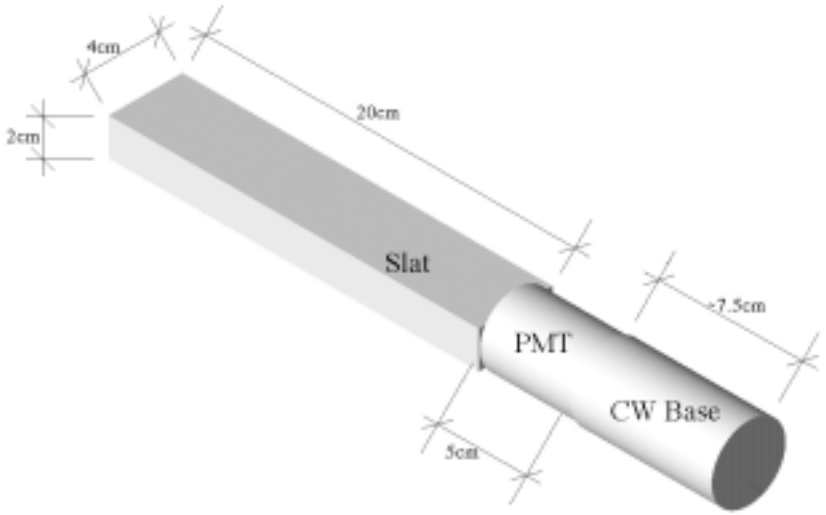

Figure 10: A slat assembly for the present system.

These assemblies are very similar to those planned for the full STAR TOF system. The main difference in the slat assembly design between the present patch and the full system concerns the lengths of the slats. In the full system, the slat lengths are chosen so that each subtends equal fractions of pseudorapidity, *i.e.* each slat subtends $\Delta\eta$=0.1. These slats thus range in length from ~21 to ~29 cm. This was chosen so that the rapidity breaks in the TOF system overlap perfectly with the rapidity breaks in the EMC towers which would sit immediately outside the TOF barrel. The analyses of the (full system) TOF and EMC data is thus simplified and certain interesting particle ratios can be calculated at the trigger level. For the present patch of TOF however, such a definition of the slat lengths is both unnecessary and relatively more expensive. The majority of the EMC will not be installed in the early years of STAR. If the RICH is approved, the present TOF patch would be installed so as to partially overlap the RICH acceptance, which anyway rules out the existence of an EMC module behind the TOF patch. The cost and time to fabricate ten groups of five slats, each of different lengths, exceeds significantly the cost and time to fabricate one group of fifty slats of the same size. The design of the mechanical support for the slat assemblies inside the tray is considerably more complicated if the slat assemblies are of ten different dimensions. Finally, the correction and analysis of the data from the system is made more complicated if there are ten different kinds of slats instead of just one - each group of slats will have a slightly different performance. The only consideration opposing the choice of equal-length slats is the expectation, given the wide plateaus in particle rapidity spectra predicted by all present models, that the average slat occupancy will then depend on the rapidity. This effect can be dealt with

offline and is minor compared to the cost, mechanical, and analysis complications associated with "equal-y" slats. Thus, the slat assemblies for the presently proposed patch are made from scintillators of only one dimension.

The various components of slat assemblies, and the completed assemblies, will be tested and graded extensively before final installation in the system. This testing will be done using an existing CAMAC-based data acquisition system that is read out via a GPIB interface to a PC.

3.2.1 Scintillator

While only a single manufacturer sells plastic scintillator slats appropriate for the present system, there are a number of choices. The chemical formulation of each affects the signal magnitudes, the signal linear attenuation length, the various light emission time constants, and the cost for specific dimensions. The options are described in this section.

The performance of a number of types of scintillators was compared in beam and described in Ref. [20]. Tests of the single-ended shingle geometry at zero magnetic field were done in the M-11 beam line at TRIUMF with a minimum ionizing beam of 300 MeV/c π^- and in a 5 kG field in the MPS facility at the AGS using an 8 GeV/c π^- beam. In these measurements, each slat was read out at one end by 1 inch diameter Hamamatsu R3432 mesh dynode photomultiplier tubes.

Shown in Fig. 11 is the time resolution of slats of various dimensions of the type BC408 (left frame) and BC420 (right frame). The resolution is defined as the standard deviation of the Gaussian distribution of times measured over many events, corrected for the resolution of the start counter that was used. The resolution so obtained is thus intrinsic to the slat assembly. The points in this figure correspond to the worst-case instance of particles striking the end of the slat farthest from the PMT. Also included is the 16% increase in the time resolution due to the presence of a 5 kG magnetic field.

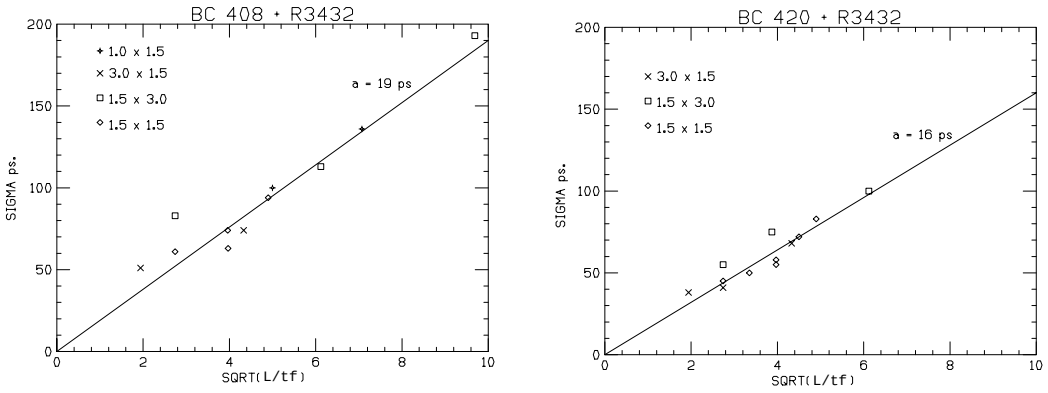

Figure 11: The dependence of intrinsic slat timing resolution on the scintillator type and dimensions as measured in beam and described in Ref. [20].

As seen in both frames of Fig. 11, the data for each chemical formulation is linear versus the quantity, $\sqrt{L/tf}$, where L is the length of the slat, t is the scintillator

thickness in cm, and f is the fraction of light collected by the spatial overlap of the scintillator end and the face of the PMT photocathode. The slope of these distributions is 19 ps for BC408 and 16 ps for BC420.

The empirical formula and the slopes measured in beam allow the prediction of the intrinsic slat time resolution expected for BC408 or BC420 slats of arbitrary dimension. These predictions are shown in Table 3 for several slat dimensions appropriate for the present system. The time resolutions include the 16% poorer performance due a 0.5 T field, and are the predictions for the worst case of hits at the far-end of the slat. Also shown in this table are other characteristics of the scintillators as quoted by the manufacturer [21].

Table 3: A comparison of various aspects of the scintillators considered. The linear attenuation length of the signal along a slat is given by λ_X, the signal rise time (10% to 90%) is RT, while the time constant for the light emission is given by λ_t. These quantities were obtained from Ref. [21]. The quantity σ_t is a prediction for the slat assembly time resolution based on the test beam data published in Ref. [20]. The final column is the cost per slat, also obtained from Ref. [21].

Name	size (cm)	λ_X (cm)	RT (ns)	λ_t (ns)	σ_t (ps)	cost \$/ea.
BC408	4×1.5×20cm	380	0.9	2.1	101	54.60
	4×2.0×20cm				89	57.40
	4×1.5×25cm				117	59.03
	4×2.0×25cm				100	62.26
BC418	4×1.5×20cm	100	0.5	1.4		81.40
	4×2.0×20cm					93.14
	4×1.5×25cm					89.66
	4×2.0×25cm					103.07
BC420	4×1.5×20cm	110	0.5	1.5	85	60.95
	4×2.0×20cm				75	65.87
	4×1.5×25cm				95	66.29
	4×2.0×25cm				84	71.91

The data shown in Table 3 allow the proper choice of the scintillator type for the present system. The formulation BC408 has a very long attenuation length, but the time constant for the emission of scintillation light is relatively long, leading to a longer rise time of the signal, and the expectation of poorer timing performance. This is confirmed by the relatively poorer intrinsic resolution, σ_t, calculated using the in-beam data as described above. For a specific slat dimension, the cost of BC408 and BC420 is similar, so the relatively poorer intrinsic performance of BC408 compared to BC420 eliminates BC408 from consideration.

The formulation BC418 was not studied in beam in Ref. [20]. The fact that the attenuation lengths, rise times, and light emission time constants for BC418 and

BC420 are similar would imply that the overall performance of BC418 and BC420 slats should also be similar. However, BC418 is generally ∼50% more expensive than BC420. The chemical formulation that achieves the best intrinsic time resolution at the lowest cost is thus BC420.

In the full STAR TOF system, the scintillator thickness is 1.5 cm. However, it is apparent from Table 3 that the overall performance improves by 10-15% by going from a thickness of 1.5 cm to 2 cm. There are no mechanical constraints that rule out this change. The chosen scintillator formulation and dimensions is thus 4×2.0×20cm BC420, for which the intrinsic time resolution expected in the STAR magnetic field for hits at the far end of the slat is 75 ps.

The empirical formula above would indicate that the slat assembly intrinsic time resolution improves with $1/\sqrt{L}$ as the location of the hits approaches the near-end of the slat. In practice, effects such as fluor decay time constants, PMT transit time spreads, capacitance in the PMT bases, noise-induced discriminator jitter, and the time resolution on on the quantity t_0 (discussed in section 4 below), impose an limiting resolution of the order to ∼50 ps for hits arbitrarily close to the near-end. Similar limits will exist in the present system. Thus, we expect the intrinsic time resolution of the present slat assemblies to vary from ∼50 ps to ∼75 ps depending on the location of the hit along the long axis of the slat as the square root of the distance from the PMT. The slat assembly time resolution averaged over the hit position would be $\sim\sqrt{50 \times 75}$, or 61 ps.

This hit position dependence can of course be exploited off-line using the locations of slat hits measured by extrapolating TPC tracks to the TOF system. It will be shown in section 4 below that the accuracy of this extrapolation is good - having a standard deviation of ∼2 mm along the direction parallel to the long axis of the slats (roughly the STAR Z axis) for momenta above ∼0.4 GeV/c. Thus, it will be possible to form samples of events gated on the position of the hit along the long axis of the slat, allowing one to look at particle spectra obtained with a slat resolution near ∼50 ps. This could be used to form cleaner samples of TOF-identified particles out to slightly higher momenta, at only the price of a lower rate.

The scintillator wrapping will consist of one layer of unpainted Tyvek 1056D, which is a highly reflective paper-like material made from spunbound olefin, and one layer of black photographer's plastic to make each assembly light-tight. As in the CTB system, simple masks in the scintillator wrapping can result in improvements in the spatial dependence of the response of slat assemblies.

3.2.2 Transducer

There are three choices for the device that converts the scintillation light into an electrical signal. These are PhotoMultiplier Tubes (PMTs), Avalanche PhotoDiodes (APDs), and Resistive Plate Chambers (RPCs). In the last few years, important advances in each of these technologies have been made, so it is relevant to consider each as the one chosen for the present system.

It is now a technical reality to place PMTs directly in a 5 kG field and achieve timing resolutions that are required for TOF systems. This was made possible by

the advent of a new phototube design called the mesh dynode tube [19]. Further advances in this tube design, the proximity mesh dynode structure with the dynodes positioned near the photocathode, reduce the transit time spread (TTS) and result in a magnetic field insensitive PMTs with a single electron TTS of 100 to 150 ps. Four such tubes, Hammamatsu R3432-01, were evaluated in beam and the results were discussed in Ref. [20]. These are 15 stage 1 inch diameter tubes with an active area of 2 cm^2. The time resolution obtained in beam and a 5 kG field for a $2.6 \times 1.5 \times 23$ cm BC408 slat varied from $\sim$60 ps near the phototube to $\sim$100 ps at the far end.

This proves that the required resolution can be obtained with mesh dynode PMTs. This technology also has the advantage of being extremely common to TOF systems. No additional R&D on the transducer is necessary. Given the test equipment and procedures developed during the CTB construction, the commissioning of the slat assemblies will be rapid and successful.

APDs are silicon semiconductor detectors. A reverse bias across the electrodes produces a depletion region, and a large electric field at the PN junction. The scintillation photons enter the device and produce numerous e-hole pairs. The electrons drift across the depletion layer towards a high field region, where impact ionization produces more pairs. APDs can operate in two modes depending on the bias voltage - the linear mode or the Geiger mode. For fast timing, the Geiger mode is generally necessary [24], which is obtained by overbiasing the diode. APDs are both smaller and cheaper than mesh dynode PMTs.

Certain aspects of the timing performance of APDs have been studied in STAR [23]. Using a ^{106}Ru source, a timing resolution of 60 ps was obtained. However, the decay electrons from the Ru source were detected directly in the APD, not in a scintillator attached to an APD. The only APDs available for these studies were red-sensitive and very small area (25 mm^2). Both aspects are quite inappropriate for the present purposes. Recent developments in industry are aimed towards APDs that are closer to blue-sensitive and larger area, but large area APDs also have a higher capacitance, which worsens the fast timing performance. As in other silicon detectors, the noise level depends very strongly on the local temperature. This temperature dependence can be ameliorated somewhat by using thermocouples to measure the local temperature and feeding this back to custom electronics to appropriately control the bias voltage. APDs biased through a high resistance and operated in Geiger mode typically have a recovery time of 1 μs, which is rather long. This also can be addressed by additional custom electronics which detect the onset of an APD Geiger avalanche and quickly starve the APD of bias current. While some R&D of these ideas was performed at the SSC Laboratory [25], it would be necessary to repeat this R&D for the present system to prove the viability of the concept as a whole. Given the lack of large-area, blue-sensitive APDs and the need to R&D several aspects of the necessary custom electronics, APDs are not a viable option for the present system.

Resistive Plate Chambers [26] are also an alternative, although these are both the active element and the transducer. They are single-gap, gaseous parallel plate detectors that operate in streamer/spark mode. They make use of a semi-conductive anode and of a special gas mixture to keep the discharge local, leading to reasonable rate capabilities. The spark discharges in only a limited area of the semi-conductive

anode (∼1-2 mm), while the remaining are of the anode remains sensitive. The counter operates at a pressure of 12 bar, which yields 4-5 primary electrons from a minimum-ionizing particle. The read-out is via strip lines, which allows the two-dimensional reconstruction of the spark location with resolutions on the order of 0.3 mm perpendicular, and 2.5 mm parallel, to the strip axis. A time resolution as good as 25 ps (r.m.s.) is possible for very thin gaps at twice the threshold voltage (∼6 kV), although typically there are tails that extend to 250 ps due to the discharge process itself. Gap widths on the order of 100 μm are chosen as a compromise between pulse amplitude, needed for the front-end electronics, and the desired time resolution. Such an detector operated in the FOPI experiment at GSI was shown to have a time resolution near 85 ps [26]. Versions of this detector technology are also being developed for the NA49 and ALICE experiments at CERN. A prototype for the ALICE experiment achieved a time resolution near 60 ps in a test beam.

The construction of the detector technology is relatively difficult. There are extremely tight tolerances on the gap dimensions. A very clean room with a laminar flow module is necessary for the fabrication. Very specific glass coatings and gas mixtures are needed to achieve the necessary performance. These and other difficulties involved in the construction the detector itself and the short amount of time until the turn on of RHIC rule out this technology for the present system.

We thus arrive at mesh dynode PMTs as the only proven technology for achieving the necessary fast timing performance under the time and financial constraints. The Hamamatsu Corporation was, until recently, the only supplier of these tubes. Within the last month, a CRADA involving BNL, Rice University, and Burle Industries was approved for the development of low cost proximity mesh dynode PMTs by Russian industry. Early versions of these cheaper mesh dynode PMTs were tested [27] and about half met the performance specifications. Unfortunately, this CRADA is not expected to produce a significant number of these tubes within the time scale required for the present system.

Therefore, the transducer proposed for the present system are proximity mesh dynode PMTs purchased from the Hamamatsu Corporation. Forty-five such PMTs are necessary in total. These are the R5946 model, which are 16 stage, 1.5 in diameter PMTs, which cost $1234 each in late September 1998. The cost estimate for these PMTs shown in section 5 will be corrected for the Dollar/Yen exchange rate as of the submission date of this proposal. It may not be necessary to order forty-five of these tubes. The same PMTs are used in the CTB, and eight of these tubes are expected to be left over after all 125 trays of CTB are completely constructed. The remained thirty-seven would be purchased from Hamamatsu with a lead time of approximately two months.

The added thickness of the present slats will allow the scintillator/PMT glue joints to be very strong without additional strain relief. The glue of choice is Epotek 301 Optical epoxy.

3.2.3 Cockroft-Walton Bases

To avoid excessive heat load and long high voltage cable runs, the dynode voltages for each phototube is provided by a 16 stage Cockcroft-Walton (CW) high voltage supply capable of operating in the 5 kG magnetic field. Shown in Figure 12 are existing CW bases. The upper one is the design circa 1996 which was used in CTB trays during the early system tests at LBL. A design decision was made for that first version to include a track and hold feature which caused the bases to trip more often than necessary. This track and hold feature does not exist in the present version of the base. The lower base in Figure 12 is the present version, which has three printed circuit boards (PCBs), not five, and about half the components compared to the first version. These bases have been run over periods of months without failure.

Figure 12: The version of the CW base produced for the twenty early CTB prototype trays (upper), and the present version (lower) which has 2 fewer PCB boards and about half the components of the CTB version.

A very mature electrical design of these bases thus exists, which is shown for the present design in Figure 13. The output is DC in the range from -200 to -2500 V. The output current is 300 μA permanent, which is equivalent to a train of 100,000 pulses/second with a 5 V amplitude into a 50 Ω load. The voltage stabilization is 0.02%. The voltage control and read-back is via a 0.2 to 2.5 V DC Voltage. The supply voltage is $\pm$30 V DC. The power consumption is 1/3 W per base. The bases are controlled via the standard STAR HDLC interface as described in section 3.4 below.

For the present system, no changes to the electrical design are necessary. However, it is appropriate to repackage these circuits to minimize their size and thickness along the trajectories of STAR tracks. The present design exists as three circuit boards which are each parallel to the long axis of the scintillator slat. The repackaging is straightforward and will result in five circular planes of circuit boards which are perpendicular to the plane of the slats. This will reduce the length of the base from

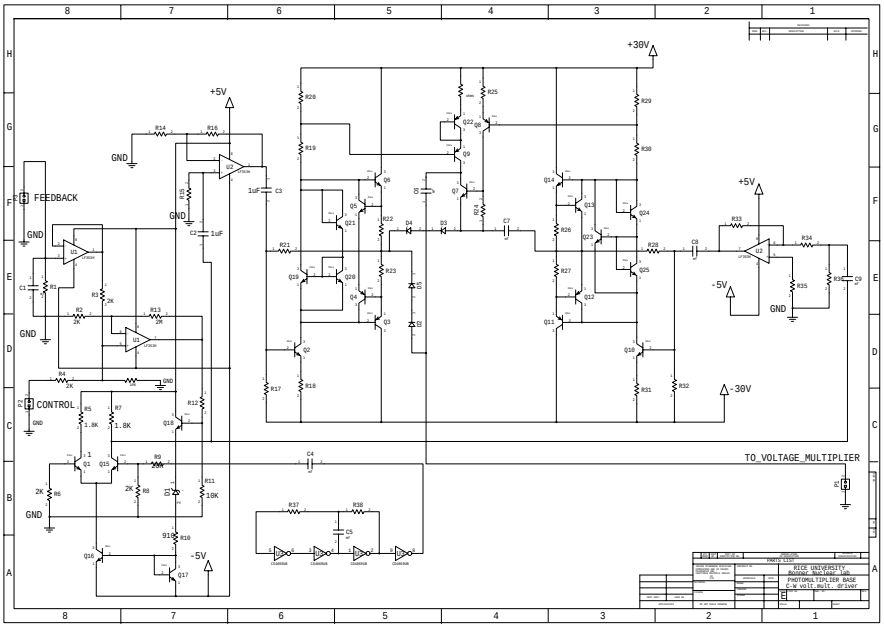

Figure 13: The circuit diagram for the Cockroft-Walton bases constructed and fully debugged for the CTB.

$\sim$6 in to $\sim$2.5 inches. The base is housed in a thin aluminum tube the same diameter as the PMT and also $\sim$2.5 inches long. This provides HV isolation for safety and radio-frequency suppression from the switching transients.

The construction time and cost is estimated as follows. The PCB design will take 100 hrs at a cost of \$30 per hour. This simply a repackaging of a mature electrical design. The parts for fifty bases cost \$2,600, and the PCB manufacturing will cost \$1,500, or \$82 per base for the boards and components. The PCB stuffing will take roughly two hours per base which, at an assumed cost of \$15 per hour, totals \$1500. Fifty bases will take two months to construct.

3.3 Trays

A "tray" is simply a long box within which the slat assemblies and on-board electronics are contained. Various plastics were originally considered for this shell for both the CTB and the full TOF system. A welded aluminum design [28] was found to be more mechanically sound, more apt to the various tolerances, more hazard safe, and negligibly more massive than the various plastic options. The wall thickness is 50 mil. This design was chosen for the CTB, presently under construction, and is thus proposed for the mechanical housing for the present TOF system. Spare CTB trays exist and one of these would be devoted to the present system.

A tray is is 2.4 meters long and 21 cm wide, and subtends one unit of rapidity and $\sim$0.1 radians in azimuth. It is inserted from one end of the magnet onto existing support rails which are glued onto the TPC outer field cage. In the full STAR TOF system, a tray is filled with 50 slat assemblies in five rows in azimuth ($\Delta\phi$=0.019) and ten rows per unit of rapidity ($\Delta\eta$=0.1).

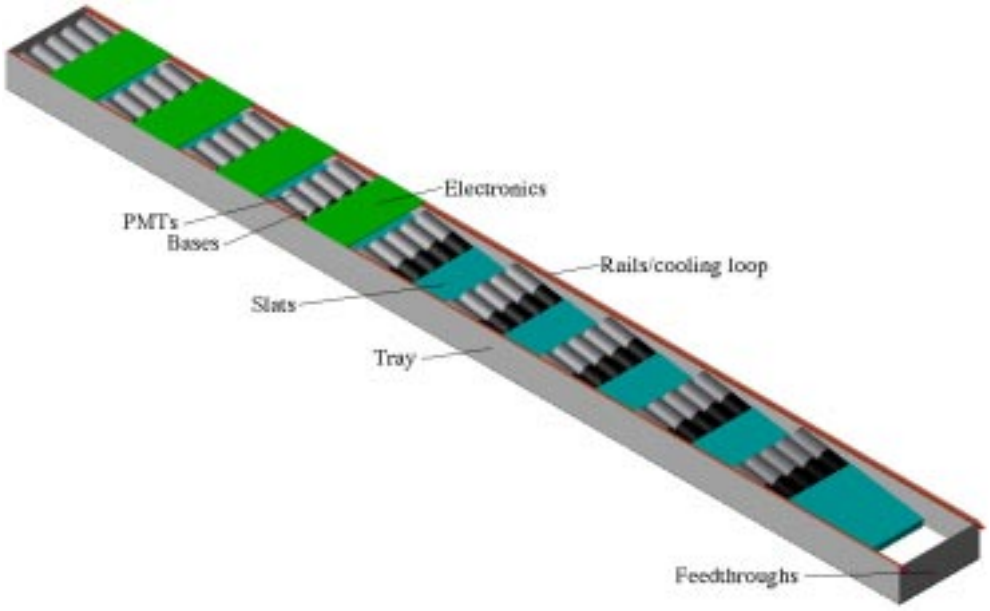

Figure 14: The arrangement of slat assemblies inside the tray. There are nine rows of five slat assemblies each. Five of the nine discriminator/CW control boards and the HDLC interface board are not shown for clarity.

In the present system, we propose filling the tray with nine rows of five slat assemblies each. There are several aspects of this arrangement that differ from design of the full TOF system. First, there is the move from equal-rapidity to equal-size slats that was discussed in section 3.2. Second, the row at the outer end is removed, resulting in nine rows of five slats instead of ten rows. This is to allow a conservative amount of room for the HDLC interface board (described below) and the numerous feedthroughs to the outside world at the tray end. This was also done so that the total number of electronic channels in the system is less than 48, which matches well with the digitization scheme of choice described in section 3.6. Third and finally, the slat rows in rapidity are projectively displaced by $\sim$1 cm. In the design of the full TOF system, care was taken to position the slats so that, projectively, the ends abut exactly to insure there is no regions in rapidity that are not covered. Here, the slats are displaced in rapidity slightly to fully insure that single tracks do not follow trajectories in rapidity that intersect two different slat rows. This also somewhat simplifies the mechanical support for the slat assemblies by loosening the tolerances within which the slats must be positioned inside the tray. As shown in Figure 15, there are thus 45 single-ended slats of equal size which have a coverage with extrema at η=0.066 and η=0.946. The phi coverage is approximately $\sim$5 mm short of the full width of the tray (21 cm) at a radius of $\sim$220 cm, or $\sim$0.093 radians.

Each of the 2 cm-thick slats are at an angle relative to the Z-axis of approximately 14°. Thus, the angles with respect to the slat normal that typical tracks strike TOF slats depends on η. In the first few rows of TOF slats near $\eta\sim$0, the typical angle of track incidence relative to the slat normal on the order of 10°, while this angle typically increases to $\sim$28° in the last row near $\eta\sim$0.95.

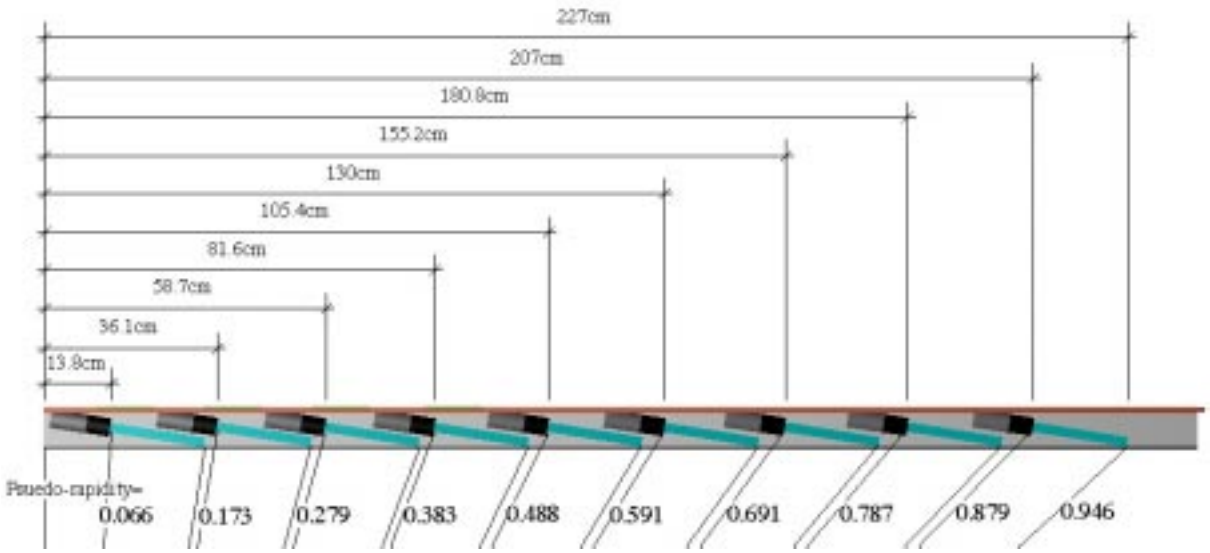

Figure 15: The side view arrangement of slat assemblies inside the tray.

Larger angles of incidence imply larger path lengths of tracks inside the slats. A 15% increase in the path lengths of typical track inside a high-η slat implies 15% more scintillation light is produced per track and hence the timing performance is improved by $\sqrt{N_\gamma}$, or about 7%. However, there is a compensating effect as well, as at larger rapidities the scintillation light is also produced over a wider range of distances relative to the slat end with the PMT. As discussed in section 4 below, the scintillation light propagation time for BC420 was measured to be 80 ps/cm, so a variation in the Z positions of the creation of the scintillation light introduces a timing spread of on the order of (80 ps/cm)*2tan(28°)/$\sqrt{12}$, or 25 ps. Typically, these two effects are a wash, although it is not difficult to investigate these questions with the experimental data. One simply studies the η dependence of the performance of the TOF system via gates on the track positions and angles with respect to the slats as measured using the tracking information.

The mechanical support for the slat assemblies in the tray is provided by the same rigid foam [29] as is used in the CTB. The is "Last-a-foam" FR-6700, which is a CFC-free, rigid, inert, flame-retardant, closed-cell polyurethane. It has a high strength to weight ratio due to its cellular structure and cross-linked resin. The density is 3 lbs/ft^3. The material is easy to work with standard milling and cutting tools.

Each tray will have water cooling for the electronics. This is provided by an aluminum cooling pipe running around the top inside circumference of the tray. This pipe is attached thermally to long aluminum angle pieces, to which the various electronics boards are mounted. The performance of this loop for tray heat removal is described in detail in section 3.5.

3.4 On-board Electronics

The on-board electronics perform the following functions. First, they are the interface between the STAR standard HDLC controls and the Cockroft-Walton bases needed

to set the voltage for each PMT in the tray. Second, they perform a leading edge discrimination of the signals very close to the PMTs that produces a very fast rise-time logic signal with low jitter relative to the time of the hit. As discussed below, this conversion to a logic signal is needed to achieve the needed fast timing performance in the presence of the long (>100 ft), and hence dispersive, signal cables. Third, it is the interface allowing the threshold applied in this discriminators to be controlled, also via the STAR standard HDLC. These functions are performed on ten printed circuit boards inside the tray - nine boards contain the discriminator and the Cockroft-Walton base control, and one board is the interface for the STAR standard HDLC bus.

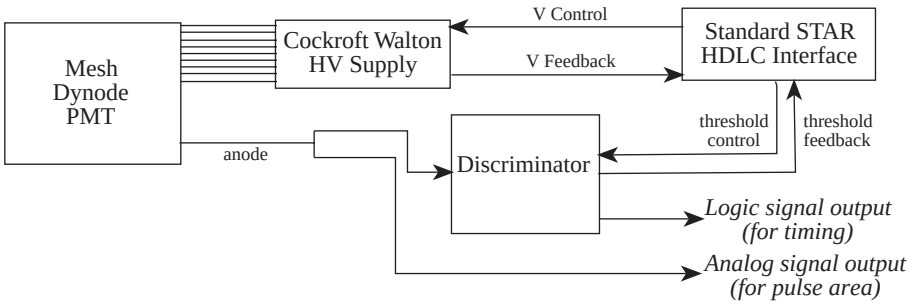

Figure 16: The various components of the on-board electronics.

A schematic view of the on-board electronics is shown in Figure 16. The output of the system is one analog signal and one logic signal for each slat assembly to be digitized on the STAR platform in standard ADC and TDC modules, respectively. The discrimination of the PMT signals inside the tray produces a very fast rise time, fixed amplitude signal that is sent out of the tray over long cables. This signal is rediscriminated near the TDCs on the platform in commercial discriminators to form the TDC stops. Such a dual-discrimination technique is common in TOF systems where long TDC signal cables are necessary before the time digitization. Examples are the TOF systems used in the BNL-AGS E802 series [30], E877 [31], and presently in E896 [32].

The primary motivation for these dual discriminator approaches is to reduce as much as possible the signal degradation due to rise time attenuation in long cables, which can be amplified if there is even a few mV of electrical noise in the system. For a scintillation time constant of $\sim$1.5 ns and a PMT rise time of $\sim$1.9 ns, the rise time of the signals out of the slat assemblies is on the order of $\sim$4 ns. After 300 feet of cable, the rise time would be increased further. For the cables proposed for the present system (described below), the rise time attenuation is specified to be <350 ps per 10 ft of cable. The rise time of the signals on the platform would thus be $<4 \oplus 10.5 = 11.2$ ns. As the PMT signal's amplitude(width) is also reduced(increased) by the long cables, the so-called "slewing" correction (described below) would be enormous for these data. Also, if there is even a few mV of noise in the discrimination of these signals on the platform, the long rise time and the noise level combine to introduce a form of jitter in the time the signals cross the discriminators on the platform. Assuming the signal is 500 mV deep, the time spread due to N mV of noise and a

signal rise time of λ_t is approximately $\lambda_t N/500$. Thus, 1 mV of noise introduces a timing jitter in the on-platform discriminators of ~20(30) ps if the signal rise time at the platform is 10(15) ns. For smaller signals, or longer cables, this jitter becomes worse, eventually ruining the performance of the system.

To combat this, the typical [30] [31] [32] approach is to discriminate the timing signals as close as possible to the PMTs. One therefore sends over the long cables signals with a fixed amplitude and a much smaller rise time of ~750 ps (shown below). This suppresses the effects that noise and the rise time attenuation in the cables have on the timing performance. As the signals to be rediscriminated on the platform all have a fixed amplitude, the stops from the second discrimination do not slew. The only slewing in the TOF times is due to the rise time versus pulse height variations after only a few feet of cable inside the tray.

The most appealing approach for the digitization of the TOF data involves cables that are ~300 ft long (as discussed in section 3.6). The quality of the noise level in STAR under actual running conditions is unknown. Thus, the conservative and proven design includes the equivalent of a discriminator for each channel inside the tray to quickly convert the signals to be used for TDC stops into logic signals. The on-board electronics also interfaces to the standard STAR HDLC bus to control the CW base output voltage and read back this voltage. Also, it sets the (single) threshold for the discriminators, and reads back this threshold. A view of the Discriminator and CW control board is shown in Figure 17. Each of these boards handles five channels, and is mounted near the PMT/base assemblies on the angle aluminum that is part of the tray's cooling loop. There are nine such boards in the tray, one per row of five slat assemblies.

The CW bases, *cf.* Figure 13, are controlled and read back via DC voltages in the range from 0 to 2.5 V. The conversion to and from the digital data produced on the HDLC motherboard is done in commercial ADCs and DACs respectively. Shown in this figure are the Maxim 147 12 bit ADC [38], and the Maxim 5253 12 bit quad voltage-output DAC [37], which both have serial interfaces. A parallel approach is also being considered. Spare channels in the ADCs and DACs are used to control and read back the on-board discriminator threshold as directed via the HDLC bus. The discriminator for each channel is single-threshold and uses one half of an Analog Devices AD96687 [33]. It is followed by a level-shifting emitter-follower to deliver the equivalent of NIM level logic signals to be sent off the tray to be re-discriminated on the platform and used as TDC stops.

According to the manufacturer's specifications [33], the propagation delay in the AD96687 is 2.5 ns and the propagation delay dispersion is 50 ps. This number is measured using square wave pulses (negligible rise time), and implies the propagation delay is 2.5 ns when overdriven by 100 mV, and 2.45 ns when overdriven by 1 V. There is no time "jitter" in the output of this comparator for pulses of a specific pulse height and zero rise times. There are, however, two sources of jitter when this IC is applied for the present system, as the pulses here have neither a fixed height, nor a zero rise time.

There is a finite width in the energy deposition and attenuation in the production of light in the scintillator and its propagation to the photocathode. This, coupled

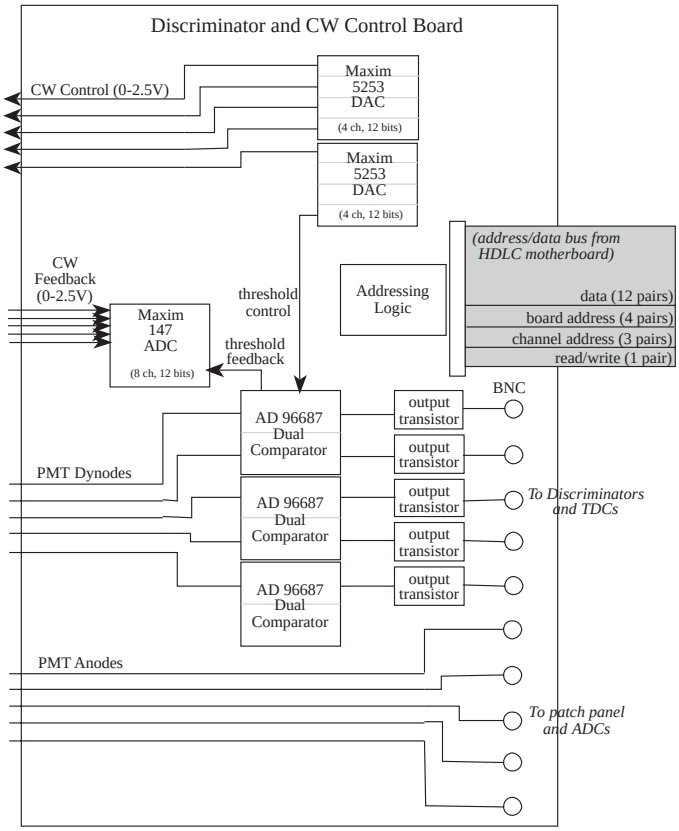

Figure 17: A schematic view of the Discriminator/CW control board.

with photostatistics in the PMTs, produces an approximately ∼15% variation in the magnitude of the PMT signals for minimum-ionizing particles (MIPs). This variation in the pulse height leads to an effective jitter via the variation in the voltage over threshold. If the mean pulse height for MIPs is 500 mV, the comparator propagation delay is near 2.475 ns. A 15% pulse height variation from the slat/PMT combination about this mean value then leads to ∼7 ps of variation in the timing of the comparator output from the propagation delay dispersion in the IC. This component is quite negligible. The second effect is "slewing," *a.k.a.* "time walk," [34] which is a dependence of the time a signal crosses a fixed voltage threshold on the rise time and the height of the pulse. This effect can be corrected for offline using the pulse areas measured by the ADCs. One fits the average slat times versus pulse areas (*i.e.* ADC values) with functions of the form t_{corr}=TDC-$a(1/\sqrt{b}\text{-}1/\sqrt{ADC})$ to determine the magnitude, a, of the slewing.[1]

The performance of such a discriminator circuit has been studied on the bench. Two prototyping rounds have already been completed. The second prototype is shown in Figure 18. For this prototype, the control of the discriminator level is done with a potentiometer that is seen in the lower left of the box. The comparator used in the

[1]This form for the slewing correction is appropriate if the shape of the leading edge of the PMT signal is parabolic. If this leading edge, for voltages near the threshold, is linear, the form proportional to $1/ADC$ is more appropriate.

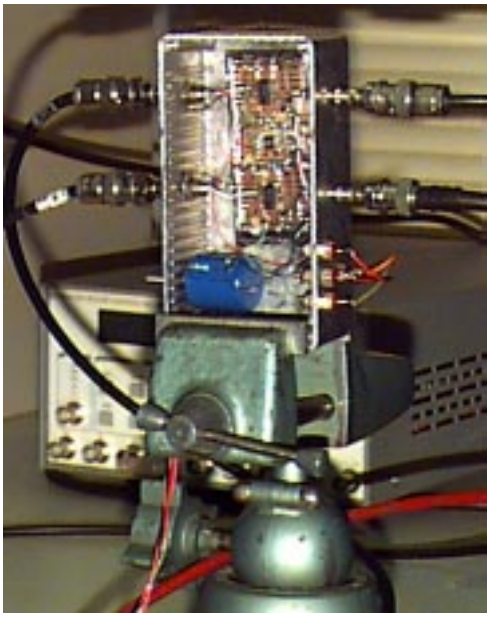

Figure 18: The second prototype of the discriminator circuit for the present system.

both prototypes is the Analog Devices AD96685, which is the single channel version of the (2 channel) Analog Devices AD96687 chips planned for the final boards. A comparator output is differential, leading to a fast rise time of the output pulses (shown below). Two differential amplifiers per channel take the comparator output and produce double-depth NIM standard logic signals.

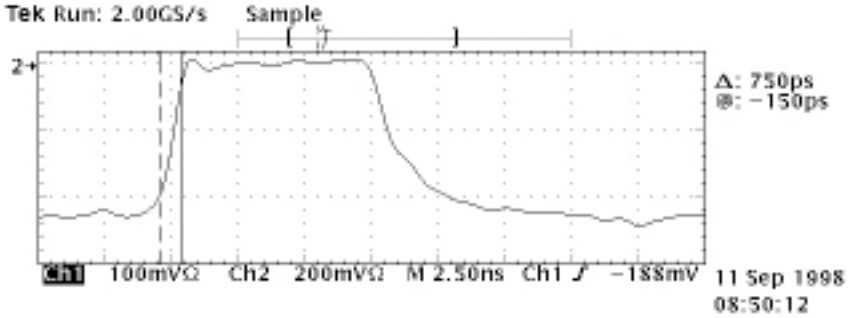

Figure 19: The inverse of the logic signal output from the first prototypes of the on-board discriminators obtained on the bench. The rise-time is ∼750 ps. The second prototype has matched rise and fall times and a flatter baseline.

Figure 19 shows the logic signal output from the first prototype board. The rise-time was 750 ps. This is faster than the performance of various NIM and CAMAC discriminators, which typically have 300 MHz oscillators and output logic signal rise times that are thus on the order of a few nanoseconds. A measurement of the jitter of the present discriminator circuit was also attempted, although the accuracy of this measurement was limited by the clock speed of the fastest oscilloscope that was available. However, the manufacturers specifications on the propagation delay dispersion, discussed above, imply this jitter is negligibly small. The second version

of this discriminator circuit, which is shown in Figure 18, has a faster fall time and a flatter baseline.

The time to fabricate and cost estimates for these electronics boards are as follows. For the discriminator and Cockroft-Walton base control, the costs per board are \$95 for components, \$100 for the PCB, and \$60 for labor and testing. Assuming 30 hours of layout time at \$30/hr, there is \$900 for PCB layout, as well as a \$1000 drop charge for the PCB fabrication. We will construct eleven of these boards (two spares), so the total cost is \$4705. A total of two months is required for fabrication, based on 2 weeks for engineering, 1 week for layout, 3 weeks for PCB fabrication, and 2 weeks to stuff and test. This work can be done in parallel with the CW base fabrication.

The HDLC interface is performed on a separate board which controls all nine discriminator/CW control boards. For this, the cost is \$100 for components, \$300 for two HDLC mezzanines, and \$1100 for the PCB. Assuming 30 hours of layout time at \$30/hr, there is \$900 for PCB layout. The total cost of this board is this \$2400. The fabrication of these boards can also be done in parallel with the fabrication of the bases and the discriminator/CW control boards.

3.5 Connections

Connections between the tray end and the outside world are needed to provide the low voltage for the CW bases, to retrieve the analog and logic signals from each slat assemblies, to control the CW bases and the discriminators via the HDLC bus, and to remove the heat generated by the on-board electronics. These connections are described in this section. An overall view of the tray connections is shown in Figure 20.

The tray design includes 3/8" diameter pipe that carries water around the circumference of the tray near the top. This pipe is attached to angle aluminum which provides thermal conductivity between the pipe wall and the various electronics boards to remove the heat generated by the electronics. The forty-five CW bases are 1/3 W each, and the forty-five channels of comparator circuits on the nine Discriminator/CW control boards are 1/2 W per channel - totalling a total of $\sim$0.85 W/channel and $\sim$40 W for the tray. It is important to keep the temperature in the tray lower than $\sim$110 °F, as the plastic scintillator becomes mechanically unstable at temperatures near $\sim$140 °F. To remove heat from the tray interior, two hoses are necessary, one delivering warm water to the tray and one removing the warmer water that has passed through the tray's cooling loop.

Bench tests were done in 1995 to measure the effectiveness of this design. At this time, it was thought the power generation TOF trays would be 2-4 W per channel. A full size tray was outfitted with the cooling loops attached to angle alumimum, to which a 1/16 inch thick aluminum plate was attached running the entire length of the tray. Twenty-four resistors were epoxied to this plate evenly along to length to generate a total power of 210 W. Water was brought to and from the cooling loop via 1/8 inch diameter tubing. The flow rate at the exit of the second 1/8 inch diameter tube was measured with a calibrated beaker and a watch. With a manometer, it was found a pressure of 2.6 psig was required to produce a flow rate of 0.1 gpm. The flow

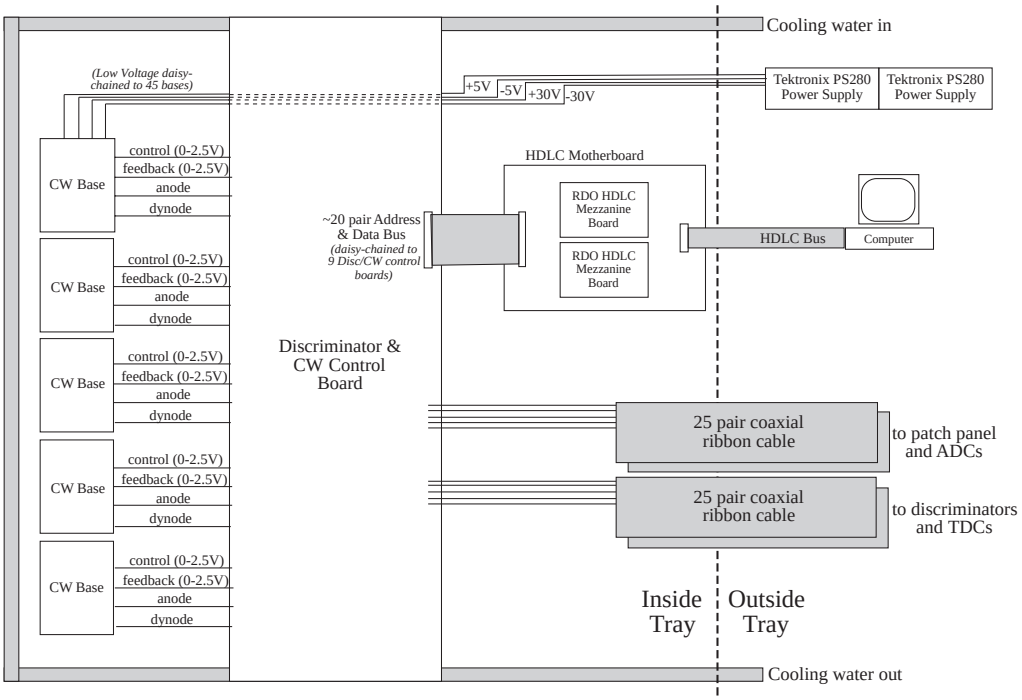

Figure 20: A diagram of the various connections between the tray and the outside world.

resistance was due almost entirely to the 1/8" tubing before and after the cooling loop that was used in this test.

After some hours for the tray to reach thermal equilibrium at 210 W, the temperatures inside the tray were measured with thermocouples and the exit water temperature was measured with a thermometer. For an input water temperature of 65.3 °F and an ambient temperature of 73 °F, the exit water temperature was 77 °F. The temperatures measured inside the tray ranged from 81 to 93 °F depending on the location of the thermocouple on on the resistor plate. Thus 210 W of power raises the internal temperature of the try to ∼20 °F above the ambient temperature. Note the heat sources for this test are more like a series of point sources than is likely with the actual electronics, leading to larger thermal gradients in this test than would be expected in the real environment. Even so, this test implies ∼0.1 gpm of water flowing through the cooling loop will limit the temperature rise inside the present 40 W tray to ∼4°F above the ambient temperature. This present system thus has quite modest requirements on the cooling water that is supplied by the STAR water system. The requirements should be low enough to allow the necessary cooling pipes to be simply "T'd" into the existing water system for the TPC.

The electronic feedthroughs are the end of the tray are the following. There are four ribbon cables that carry the analog and logic signals from the tray to the platform. Another ribbon cable is the HDLC bus used to control and monitor the total voltage output by each of the CW bases, as well as the (single) discriminator level. Finally there are the wires that provide the low voltage for the CW bases.

The signal cable [35] is shown in Figure 21. Four of these ribbon cables, each 25

conductors (or 2.5") wide , will bring the analog and logic signals from the tray to the platform. Each consists of individual solid conductors, each with foamed polypropylene insulation, a foil shield, and an oriented drain wire. An extruded contoured outer jacket allows mass termination or separation and stripping of conductors. The thickness is 0.1" nominal, the impedance is 93 Ω, the propagation delay is 1.35 ns/ft, and the attenuation is 6 dB/100 ft at 100 MHz. We choose 93 Ω ribbon cable over 50 Ω ribbon cable as the attenuation is a factor of two less in the 93 Ω cable.

This implies that 43 Ω series resistors will be necessary in the patch panel on the platform to match the 50 Ω input impedance of the ADC modules. As 60 and 720 Hz noise components in even carefully defined experimental grounds are typical at the AGS, we are also considering a version of this panel that would include >1 MHz bandpass filters ($2 each) on a simple PCB to remove any low frequency noise components.

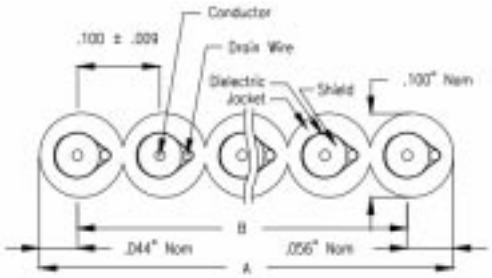

Figure 21: The cross-sectional view of the coaxial ribbon signal cables.

The low voltage for the CW bases is provided by power supplies that are located in racks on the platform. Two power supplies are needed to provide the ±5 V and ±30 V low voltage. These supplies are the Tektronix PS280 DC Power Supply [36], which each cost $800. Four ∼100 ft long 20 gauge wires connect these two power supplies to the tray.

Finally, the CW base control, CW base monitoring, and discriminator threshold is done via the STAR standard HDLC bus. This is a 5 pair ribbon cable, which attached inside the tray to a HDLC motherboard, upon which 1-2 standard RDO HDLC mezzanine boards are mounted. As only 1-2 mezzanine nodes will be needed for this system, we assume it will be possible to connect to a spare channel of an existing Radstone board. The system from this point onward, including the user interface, would thus be the STAR standard, so no development funds or effort are needed for these parts of the slow controls interface.

3.6 Digitization

The single tray in the present system provides analog and logic signals that are to be digitized in ADCs and TDCs, respectively. The ADCs provide pulse area information that indicates the number of particle hits per slat. The pulse area information is also related to pulse heights via the individual PMT line shapes. This information is needed for the slewing correction of the times the PMT signals cross the on-board leading edge discriminators. The logic signals are rediscriminated on the platform

and then sent to high resolution TDCs to provide the timing information. In this section, we comment on the various aspects of this digitization of the analog and logic signals from the tray, and how the digital data is inserted into the STAR data stream.

The CTB and EMC are "fast" detectors compared to the TPC, so provisions are being considered for these systems that allow the collection of single-detector data only in a fast path to tape. This rapid collection of data from these systems is intended so that high statistics spectra can be collected to allow informed choices for trigger thresholds. The present system is also a "fast" detector, yet the information it provides in an event is no more useful than that from the CTB unless there is tracking information from the TPC in the same event. There is thus no requirement for a "fast" TOF-only data stream.

The time digitization requires start and stop signals. If the TDCs are operated in common start mode, the stops are provided by the present system and the starts are obtained from some other source in STAR. The preferred system to provide the start signal is the VPD, which is capable of providing a high resolution start signal after correcting for the location of the primary vertex in each event. However, there is no plan at present to build the VPD in the first, and possibly in the first two, years of of RHIC running [39]. The next best option would be the ZDC. This detector has a poorer time resolution of $\sim$250 ps [40], although the effects that such a start resolution has on the TOF measurements can be corrected for offline as described in the next section.

It is not clear if TDCs are planned for the ZDC time digitization. Such TDCs need not exist as far as the present system is concerned. What is needed by the TOF system is simply a NIM-level logic signal produced by the discrimination of the signals from the ZDCs. The logic signal from the ZDC will be fanned to 4-5 cables at the TOF-DAQ crate (described below) on the platform. One of these will start the TDCs, one will be start the gate generator for the ADCs, and the others will be delayed and digitized as if they were stops from TOF channels. To enhance the probability that a L0 trigger follows for starts so generated, it may be useful to logically .AND. the ZDC logic signal with some minimal requirement on the CTB multiplicity. It is expected that the time needed to form such a coincidence is negligibly larger than the time needed to form the ZDC start alone.

The amount of data produced by the system is as follows. The worst case has data in all 45 slats in an event, for which there are 45 four byte words for the ADCs and 48 four byte words for the TDCs. The three additional TDC words are for the TDC measurement of the start signals themselves described above. In total, there is thus $\sim$400 bytes of TOF data per event.

It is important to note that certain aspects of the interfaces to the STAR DAQ and Trigger systems are not entirely defined at the present time. It is felt that these gray areas, each pointed out in the discussion below, are all tractable problems. For example, the present requirements on the trigger interface are very similar to those for the proposed RICH detector. A common solution for this interface for these (and other new) detectors is presently being discussed amongst the present TOF group, the RICH group, and the STAR Trigger group, and is outlined below.

There are three technologies to be considered for the digitization: VME, Fastbus, and CAMAC. In the case of VME, a commercial TDC unit with a <50 ps resolution does not exist. However, one may use a technique that involves the "stretching" of the start-stop time interval by a factor of twenty or so, and then digitizing with a VME TDC with 1 ns resolution. This would involve three LeCroy 1275 16 channel time stretchers and three LeCroy 1176 16 channel TDCs. This technique [41] is planned for the TOF system in the BABAR experiment [42]. However, this is a complicated and relatively new technique. It is also quite expensive - three LeCroy 1275's and three LeCroy 1176's total $34,260. One would likely have to purchase the VME ADCs, *e.g.* the LeCroy 1182, as well.

Fastbus is the next alternative. High resolution TDCs are available, *i.e.* the 64 channel LeCroy 1875a, and the interface to VME can be performed with a LeCroy 1821/ECL in the Fastbus crate connected to a LeCroy 1190 Dual Port memory in VME. Such an approach is presently being used for the TOF system in BNL-AGS Experiment 896. However, Fastbus systems are overkill for a system with a low channel count, such as the present one, and Fastbus crates are not known for their reliability.

Therefore, the best choice for the digitization of the present system is CAMAC. The ADCs and TDCs are common enough that they might be easily borrowed from HEEP or another pool. Also, the crates are both small and reliable. A schematic diagram of the crate where the digitization is performed, and the interface to the STAR DAQ system, is shown in Figure 22.

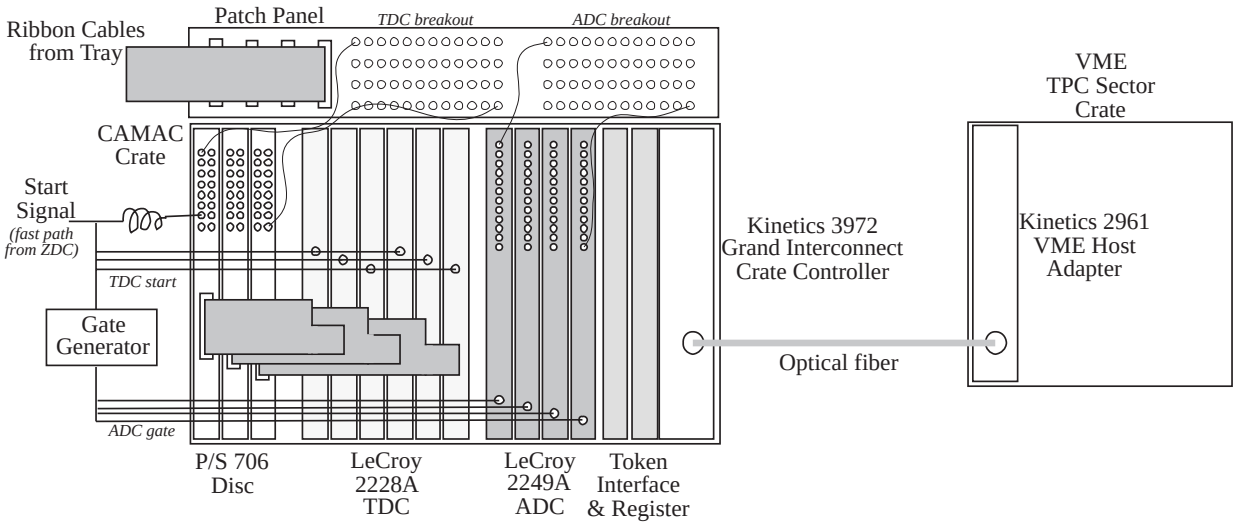

Figure 22: The components of the TOF/DAQ interface.

The four ribbon cables from the tray are broken out to Lemo connectors and impedance matched to the ADCs and TDCs in a custom patch panel. The ADCs and TDCs in this system are commercial CAMAC units that we will attempt to sign out from an equipment pool. The most common units are manufactured by LeCroy and Phillips Scientific. The LeCroy 2249A ADC is a 12 channel, 10 bit, single width unit with a 0.1% resolution and a 256 pC full scale. The input impedance is 50

Ω. Confirmation of operation and calibration is provided by a test feature which allows all twelve channels to simultaneously digitize a charge proportional to a DC level provided by a front panel Lemo connector. This model has a 60 μs conversion time and the ability to incorporate fast clears via a front panel input. The LeCroy 2228A TDC is an 8 channel, 11 bit, single width, common start unit, with a 110 Ω input impedance pin to pin, internal test functions, a 100 μs conversion time, and fast clear inputs. The resolution is 50 ps in the 100 ns full scale range, although a 30 ps resolution is available via a factory option (LeCroy 2229/400). More attractive for a number of reasons are the Phillips models. Both the Phillips ADCs and TDCs are 16 channels each, as opposed to 12 and 8, respectively. The Phillips 7186H TDC has a 25 ps/channel resolution (as opposed to 30-50 ps/ch in the LeCroy model), a 7.2 μs digitization time (versus 100 μs), and a 12 bit resolution (versus 11). The Phillips 7166 also has 12 bit dynamic range (versus 10), and a 7.2 μs digitization time (versus 60 μs).

Assuming start/stop timing is adjusted so that the fastest particles land in channel $\sim$400 of the TDCs, this implies roughly a factor of 5(10) dynamic range in the time interval measurement in the 11(12) bit TDCs. The absolute time of flight for the fastest particles near η=0 is on the order of 220 cm/(30 cm/ns), or $\sim$7 ns. A factor of $\sim$5 dynamic range thus implies the TDCs overflow if the time of flight exceeds $\sim$35 ns. For a 2.2 m flight path, this implies the lowest values of the track velocity, β, with non-overflowing TOF TDCs is $\beta_{min}\sim$0.21 ($\gamma\sim$1.023). Thus, the TDC dynamic range implies low momentum cut-offs in the TOF measurement near η=0 of on the order of $\sim$0.03 GeV/c, $\sim$0.1 GeV/c, $\sim$0.2 GeV/c, and 0.4 GeV/c for π, K, p and d, respectively. Thus, the TDC dynamic range has little effect on the lowest momenta with direct TOF PID for pions, kaons, and protons, as for these it takes transverse momenta above 220cm/2/[0.0003*B(kG)], or $\sim$165 MeV/c, just to reach the radius of the TOF system. The momentum lower limit for deuteron PID imposed by the dynamic range of the TOF TDCs is by chance the same as the lowest deuteron momenta at which the 10 bit-equivalent ADCs for the TPC dE/dx overflow.

The interface to DAQ is also not entirely defined at this point, although discussions with the STAR DAQ experts [43] have resulted in the following general design. The communication to VME would proceed via a Kinetics 3972 Grand Interconnect Crate controller in the TOF CAMAC crate, and a Kinetics 2961 Host Adapter in a DAQ VME crate. This VME crate could be a TPC sector crate, in which case the token interface may be simplified and the TOF system could participate in the STAR Level-3 trigger. The crate controller and the host adapter are connected via optical fiber using connectors on the front panel of each module. This satisfies the requirement that copper is not used to connect the TOF crate to the DAQ system. The Kinetics 3972 CAMAC crate controller costs \$9400 with a 8 MB buffer. The Kinetics 2961 host adapter costs \$7345. For both items there is a 6 week delivery time.

The timing is generally as follows. Approximately 300 ns after a collision a fast signal from the ZDC is available at the TOF crate on the platform. To reduce background rates and hence enhance the chances that a L0 accept will later come for this event, it may be useful to start to TOF digitization with a signal that is an .AND. of the ZDC signal and some minimal CTB information. We assume an additional $\sim$50

ns for the NIM logic needed to generate the ADC gates and TDC starts. The coaxial ribbon cables that connect the tray and the patch panel on the platform will thus be approximately 300 feet long, which brings the tray's analog and logic signals to the platform approximately 400 ns after the collision. The re-discriminated logic signals and the analog signals are then digitized in the TOF CAMAC crate.

The completion of this digitization generates a LAM signal which instructs the crate controller to execute from an internally stored list of commands to read out all $\sim$100 channels of ADC and TDC in the crate. Events are stored in an indexed way in the 8 MB list memory of the crate controller. If a token arrives on the CAMAC dataway after $\sim$1.5 μs, the crate controller will read the register and save the token with the event data in the controller list memory. If a L0 accept is not seen, or one is seen but there is later a L2 abort, the event is flushed locally. If, however, a L0 accept is seen for this event, and a L2 abort is not seen later, the TOF crate pokes the DAQ system by generating a VME interrupt.

At this point the STAR DAQ has been instructed that the TOF crate has data it would like be read from the crate controller over the optical fiber to one of DAQ's VME crates. At its leisure, the DAQ system reads a small header for the event in the crate controller memory to determine the token number for the event(s) sitting the list memory. If after the L3 decision DAQ decides to archive the event, DAQ will then grab the TOF ADC and TDC data from the TOF crate. The manner in which this VME interrupt is generated not fully designed at this point.

An interface to the STAR trigger system is thus necessary so that a token can be assigned to each TOF event and so that L2 aborts can be received by the TOF crate to flush events from the local memory. This interface is not fully designed at this point, although there are similar needs for the RICH system, and a general interest amongst these groups in a common solution. The present thinking in the trigger group is the following. A "generic" mezzanine card for the Trigger Clock Distribution (TCD) boards would be developed by the Trigger group. Such a board recognizes a specific action word or set of action bits to decide if a subsystem is to be involved. It then packages the token bits into a 16 bit word with any subsystem specific action bits and makes it available on a 34 conductor twist&flat cable. All that is needed at the detector end is an I/O register in the subsystem crate, which would be read to see what token to use for indexing and what action might be required for the event. Thus, the TOF-token interface will involve a Kinetics 3470 24-bit input register, which costs \$1,050, and a TCD board, which costs \$3,000. An additional \$2,000 is conservatively assumed for TCD mezzanine cards.

If the VME crate holding the TOF host adapter is a TPC sector crate, the TOF information can be used in L3 trigger processing. The TOF data can also be trivially provided to the trigger system for use in the L0 processing. The information on the number of lit slats in the tray in each event is calculated entirely on the platform. Each of the Phillips 706 discriminators to be used for the second discrimination on the platform has a sum output which is proportional to the number of channels with a valid stop signal from the tray. The three sum signals from the three platform discriminators will be added at the TOF crate and sent via a single cable to the Trigger system for use in L0 decisions.

4 Simulations

In this section, several specific simulations are described which will elucidate certain aspects of the performance of the present system. The aspects considered here include the occupancy and multiple hit probabilities, the accuracy of the crucial connection between TPC tracks and TOF hits, and the offline correction for the electronic starts used in the digitization. The start correction is most accurate in high occupancy events. The last aspect discussed here thus concerns the performance of the present TOF system in extremely low occupancy events, such as in peripheral Au+Au collisions, or p+A and p+p collisions.

The simulations were done with the STAR simulations and analysis framework in the analysis shell STAF. The platform was LINUX and the STAR production release "pro" was used, which corresponded to releases SL98e and SL98h over the course of the simulations performed for the present proposal. The detector geometry definitions via the Advanced Geometry Interface, and the GEANT implementation, GSTAR, are part of the analysis shell via dynamic binding. The standard definitions of the various STAR detectors was used. A Year-1 configuration of the mid-rapidity detectors was defined, which includes the standard beam pipe and magnet, the full TPC, and the full TOF (120 trays). The simulation of 120 trays of TOF in each event effectively increases the statistical accuracy of the present studies of the performance of a single TOF tray with no loss of generality. A uniform magnetic field of 0.5 T was used. GSTAR was run with the standard cuts and "all physics on." The events used were provided by the HIJING and VENUS models for central (b<2 fm) Au+Au collisions and were obtained from the STAR library on the mass data store at the RHIC Computing Facility.

The detector simulation was performed with the TPC fast simulator, *tfs*, and the CTB/TOF simulator, *cts*. These convert the information recorded during the GEANT event propagation at volume crossings into the digitized information expected from the actual detectors. The TPC fast simulator was run with the default parameters, while the parameters for the TOF simulator were modified as appropriate for the design of system described in the previous section. The difference is the modest improvement in the intrinsic resolution of the slat assemblies due to the choice of 2 cm thick BC420, as opposed to 1 cm thick BC408, as described in the previous section. The result of this change is a decrease in the geometrically averaged slat assembly time resolution from 77 ps to 61 ps.

The analysis was performed with the full TPC tracking code, *tpt*, including its evaluation package, *tte*. The TPC tracking was performed with the default parameters, and "open" cuts on the quality of the track reconstruction were used. Local routines based on a standard helix track model were written to extrapolate the TPC tracks to the TOF system. This local software also traverses the pointers in the various TPC and CTF tables to allow the association of TPC tracks to the event generator particle information, of TPC tracks to digitized CTF hits, and of simulated digitized CTF hits to the raw GEANT CTF crossings.

4.1 Occupancy

Certain mechanical constraints limit the arrangement and total number of slat assemblies that can be fit into a single tray. In the present system, there are nine rows of five 4×2×20 cm slat assemblies in the tray. The occupancies and multiple hit probabilities of such an arrangement for the worst-case scenario of central (b<2 fm) Au+Au events are shown in Table 4.

Table 4: The slat occupancies and multiple-hit probabilities obtained from the full simulation of central HIJING and VENUS events.

Probability per slat	HIJING	VENUS
No hits	61%	20%
1 hit	25%	26%
2 hits	9%	22%
3 hits	3%	15%
≥1 hits	39%	80%
≥2 hits	14%	50%

The occupancy and multiple hit probabilities in central VENUS events significantly exceed those in central HIJING events. This is not surprising given the approximate fact of two difference in the primary track multiplicities from these two models (*cf.* Figure 6) . In the HIJING(VENUS) events, 3/5(1/5) of the slats are not struck by a particle, and 1/7(1/2) are struck by two or more particles, primary or secondary, in each central event.

One quarter of the slats are struck only once in both classes of events. These will be identified during the analyses of real data by two means - by the extrapolation of primary and secondary tracks, but (more accurately) via the ADC information recorded for each channel in the system. This proceeds as follows. In large impact parameter events, the occupancy is very low. This allows one to form ADC distributions for each channel in the system that have negligible contributions from slat multiple hits. One then studies the evolution of these ADC distributions with increasing occupancy (*e.g.* increasing centrality) to understand the modifications of each of the ADC distributions that are caused by multiple hits. With this dependence understood, one can then make informed choices for the ADC gates used to select slats that were struck exactly once in a given event. As the raw ADC distributions are now well understood in general, the efficiencies of these ADC gates, which are needed to produce cross sections, is also well understood.

In a sense, the inability of the present system to form significant EbyE observables (*cf.* section 2.2.6) is technically an *advantage* when viewed with the physics scope of the present system in mind. Given the (small) solid angle coverage of the present system, there is thus no real need to push to a 100% acceptance for the tracks in the solid angle of the present system. The multiple hit probabilities, independent of the

model, are such that 1/4 of the slats are struck only once. These slats will thus lead to "golden" spectra with a very well understood efficiency corrections based on the ADC distributions.

From an overall rate standpoint, it is important to note that it will certainly be possible to use the timing information from slats that are struck more than once. These are again identified using both the tracking and ADC information, and will allow the formation of "silver" spectra at higher rates, but with somewhat higher backgrounds. If the experimental event sample of interest is small, *and* if the experimental track multiplicities are similar to the VENUS predictions, it may be necessary to attempt to recover as much rate as possible by allowing multiply-struck slats into the TOF analyses. Otherwise, the well-defined "golden" path to TOF-based spectra is capable of accomplishing all of the physics goals of the present system.

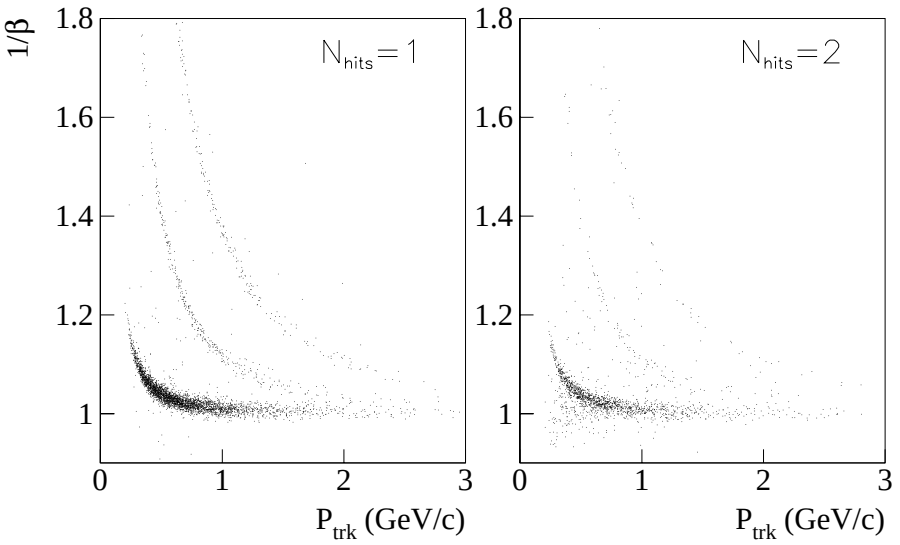

Figure 23: The inverse velocity versus reconstructed track momentum distributions for slats that are struck exactly once (left frame) and twice (right frame) from full simulations of central HIJING events.

That useful timing information can still be extracted from slats struck twice is shown in Figure 23. The left frame depicts the inverse velocity distributions versus the reconstructed track momenta for the full simulation of central HIJING events under the condition that the slat is struck only once in the event. The usual bands for pions, kaons, and protons are clearly visible. The right frame shows the same distributions, although here each point corresponds to a track that strikes a slat that, according to GEANT, was struck by two particles during the event.

There are two classes of multiply-struck slats to consider here. The first class are those multiply-struck slats for which one hit is from a TPC track and the other is due to a particle from some slower secondary process, *e.g.* albedo, which may or may not be trackable in the TPC. If the time difference between these hits is more than $\sim$1.5 ns, the timing information from the slat is exactly that for the tracked particle, and the one point in the right frame for the found track is squarely in one of the particle bands. The other class includes those multiply-struck slats with hits from

two tracked particles. Here, the momentum, total path length, and hit position along the slat's long axis are available from the TPC for both particles striking the slat. In general, it will be possible to assign the measured slat time to one of these tracks, as the other may have a momentum, path length, and/or hit position which rules out the possibility that the hit from this track produced the TDC stop under any mass hypothesis. In the present simulation and in the actual detector, the scintillation light pulse that arrives at the PMT end of the slat the earliest in a given event is the pulse that defines the time signal for the slat. Thus, in this class there are two points in the right frame, one for each track extrapolated to a doubly-struck slat. Here, the measured time of flight is exactly that for one of these two tracks, while the other track is assigned a time that is too early.

These effects lead to the "backgrounds" seen below the pion band and between the other bands in the right frame. However, the fact that the usual bands for pions, kaons, and protons are clearly visible in this frame implies that a significant fraction of the tracks exist in one of these two classes and hence are identifiable even in multiply-struck slats. The efficiencies(backgrounds) involved in such an analysis will depend on the cuts that are used and may be lower(higher) compared to analyses of singly-struck slats. Such an analysis is nonetheless a valid path towards an increased acceptance of the system, should it be necessary for a particular (small) event sample of interest.

4.2 Extrapolation

The present system does not work without the information on track momenta, positions, and path lengths that is provided by the TPC. The resolution with which each of the necessary quantities are measured by the TPC and its track reconstruction software bears directly on the performance of the TOF system. What is needed are the values of (R,ϕ,Z) where each track would strike a TOF slat, and the total path length for each of these tracks.

The measurement of the (R,ϕ,Z) for each track at the positions of TOF slats is needed both to identify the correct TOF slat that is struck by each track, but also to perform an important correction to the slat times. This correction is for the (approximately Z-dependent) propagation time of the scintillation light from the point where the track crosses the slat to the end with the PMT. This propagation time was measured in beam tests [20] and the results for BC420 scintillator are shown in Figure 24.

The propagation time of the scintillation light is 80.2 ps/cm for the formulation of choice for the present system. Over a $\sim$20 cm-long slat, there can thus be $\sim$1.6 ns of variation in the apparent time due only to variation in the positions of the hits on the slat. Obviously, one must correct for this effect. To do this, one must locate the position of the each hit along the long axis of each slat using the extrapolation of the TPC track to the cylindrical radius of the TOF system. The uncertainty in this extrapolation (in cm) thus contributes to the overall resolution of the present system with a slope of 80.2 ps/cm.

To convert times of flight to velocities at specific momenta, the total path length

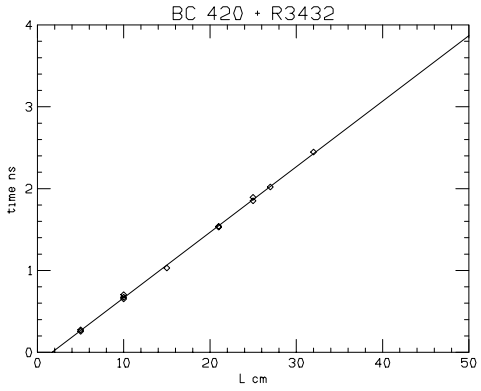

Figure 24: The propagation time of light produced in BC420 scintillators as a function of the distance along the slat's long axis from the hit to the PMT end as measured in beam and described in Ref. [20]. The slope is 80.2 ps/cm.

for each track must also be measured. For fast particles, a 3 cm error in the path length measurement skews the apparent velocities by the equivalent of a 100 ps mistake in the timing.

Full simulations were performed to determine the resolutions by which the "measured" (R,ϕ,Z) positions of tracks at the TOF system and track total path lengths reproduce the actual values for each track that were obtained from GEANT. By following pointers across STAF tables, one can associate each geant crossing in a TOF slat with a reconstructed TPC track, and vice versa. The exact position of each geant crossing in a TOF slat is passed to STAF by GSTAR/G2T. The extrapolation of each TPC track to the rapidity-dependent radius of the TOF system using a helix track model and uniform 0.5 T magnetic field provides the "measured" (R,ϕ,Z) position at the TOF system,

For the track total path length measurement, the actual values are also obtained directly from GEANT. One obtains the "measured" values by extrapolating each track to the primary vertex and locating the (R,ϕ) position of the closest approach to the primary vertex. This (R,ϕ) position and the extrapolated (R,ϕ) position of the track at the TOF system form a line segment in the bend plane. The length of this segment, C, and the circle radius for the track obtained from the tracking, R, gives the track path length in the bend plane, S_{bend}, as S_{bend}=$2R\sin(C/2R)$. The total "measured" path length in three dimensions, S, is then $\sqrt{S_{bend}^2 + Z^2}$, where Z is the "measured" value obtained from the track extrapolation.

The results are shown in Figure 25 on a logarithmic scale. The upper left frame is a scatter plot of the difference, in centimeters, between the azimuthal positions of the actual hit and the extrapolated track at the TOF radius as a function of the reconstructed track momentum. The upper right frame shows the differences between the actual and extrapolated Z-positions, and the lower left frame shows the differences between the actual and measured track total path lengths, S, both as a function of the track momentum integrated over $|\eta|$<1. The lower right frame shows the psuedo-rapidity dependence of the accuracy of the track total path length measurement integrated over all reconstructed track momenta. Each frame bears on

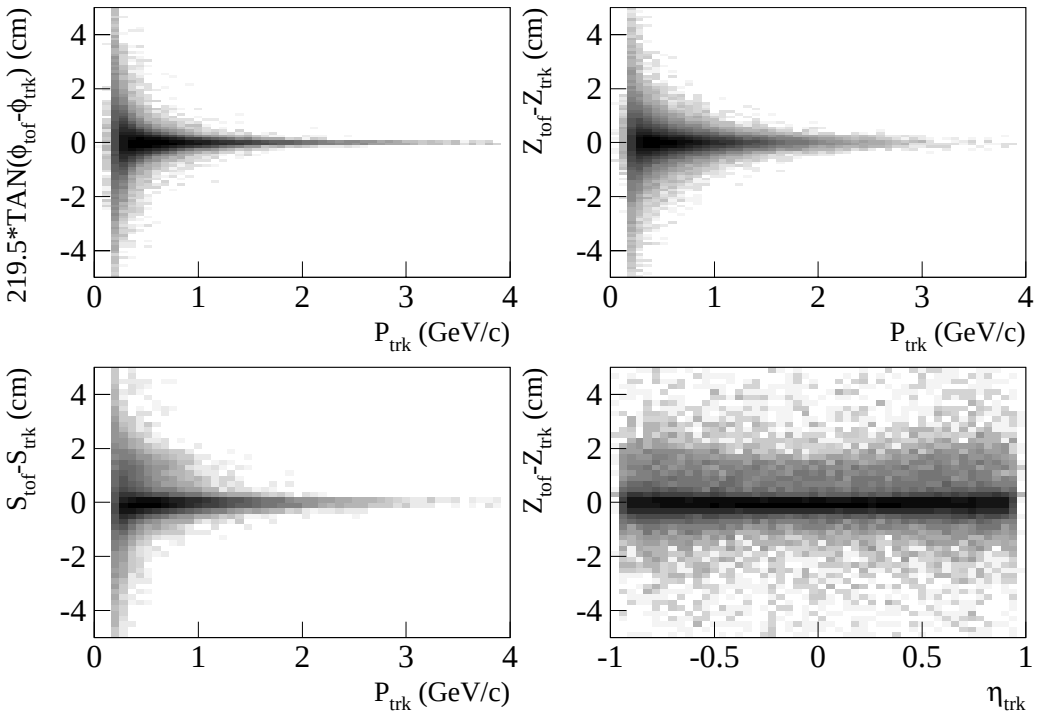

Figure 25: The difference between the extrapolated positions of TPC tracks to the TOF system and the actual positions of TOF hits azimuthally (upper right) and along Z (upper right) versus the track momentum on a logarithmic scale obtained from the full simulations. The lower two frames show the momentum (lower left) and pseudo-rapidity (lower right) dependence of the accuracy of the track total path length measurement.

the accuracy of, respectively, the proper assignment of slats to tracks, the propagation delay correction, and the velocity measurement via the track total path length.

According to Figure 25, the accuracy of the track extrapolation is generally better than a few millimeters (quantified below) for tracks with momenta above a few hundred MeV/c. The errors in the various extrapolation quantities for tracks with lower momenta can be on the order of centimeters. We note that no attempt was made to optimize the TPC tracking software or the relatively open cuts used in the simulation for the extrapolation of very low-momentum tracks. However, such difficulties in the track extrapolation at very low momenta cannot be totally eliminated. These resolutions thus form an effective *lower* limit on track momenta for which the TOF system is applicable of 0.3-0.4 GeV/c, depending significantly of course on the cuts and efficiencies one chooses to allow in a given analysis.

Figure 26 depicts the standard deviations of the differences shown in Figure 25 versus either the momentum or pseudo-rapidity obtained from Gaussian fits to vertical slices of the frames in Figure 25. For momentum above ~0.4 GeV/c, the azimuthal position of each TOF hit by a track is measured to better than ~0.1 cm at the TOF radius. This is to be compared with the 4 cm width of each slat in this direction. The Z position of each hit is measured to better than ~0.2 cm, implying that the com-

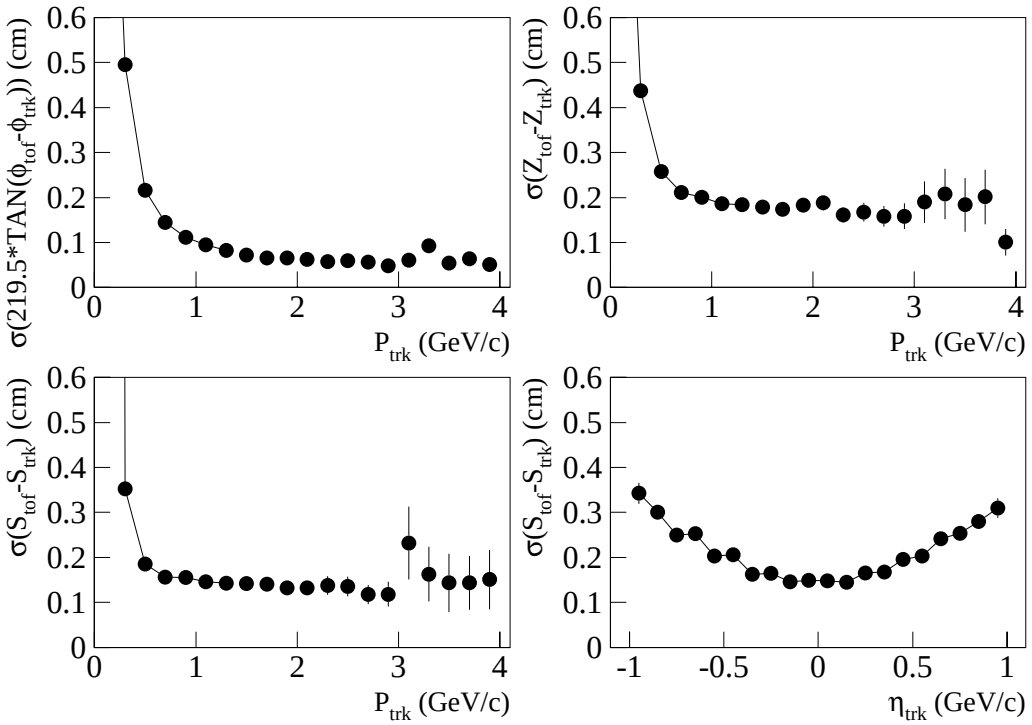

Figure 26: The same as Figure 25, except that the standard deviations, in centimeters, of Gaussian fits to the differences between the actual and measured position and track length values are shown versus the track momentum (first three frames) and the pseudo-rapidity (lower left) frame.

ponent to the overall TOF resolution arising from the correction for the scintillation light propagation time is only ∼16 ps, which is quite negligible.

The track total path lengths are also quite accurately measured by the TPC for momenta above ∼0.4 GeV/c. The errors in the total track lengths are only 0.15 to 0.35 cm for tracks with total path lengths ranging from $\gtrsim$220 cm ($\eta\sim0$) to $\gtrsim$290 cm ($\eta\sim1$). The time it takes for a 1.5 GeV/c π(2.5 GeV/c p) particle to traverse a distance of 1.5 mm is ∼5(6) ps. This implies the TPC provides the track total path lengths with a much better resolution than necessary to achieve the required resolution on track velocities.

4.3 The Quantity T_0

The quantity called t_0 is electronically either the "start" if the TDC digitization is performed in common start mode, or it is the "stop" if the TDCs are run in common stop mode. For the following discussion, we assume a common start system, although the comments made here apply in exactly the same way to common stop systems. Either way, the resolution in the measurement t_0 is equally as important as the measurement of the time a particle crosses a scintillator slat, as the overall resolution of a TOF system is the quadrature sum of these two quantities. If the intrinsic resolution of the slat assemblies is 61 ps (see section 3.2.1), and the hit position correction of

the slat times (see previous subsection) introduces and additional smearing by 16 ps, then the overall stop resolution is 63 ps. In order to meet the requirement that the overall resolution is less than 100 ps, the start resolution must be better than 78 ps. Obviously, the system performance would improve overall if the quantity t_0 can be determined event by event more accurately.

The optimum source for the t_0 signal is a detector that also has a very good time resolution, such as the VPD. However, the VPD is presently not planned to exist in STAR in the first year of RHIC, and possibly also not in the second year [39]. Therefore, for the present system, the start signal will be provided in a fast path from the ZDC. The time resolution of the ZDC has been measured in beam and is on the order of 250 ps [40]. While electronically this signal forms an acceptable start, the resolution on the t_0 provided by the ZDC cannot by any means satisfy the requirement that the overall resolution of time differences measured by the ZDC and the TOF system is less than 100 ps. Thus, it will be necessary to correct for the poor resolution of the start signal using the information from the TOF system itself. This correction and its performance is described in this section.

This correction is based on the following idea. Ignoring trivial timing offsets from cable, PMT transit time, and other electronic delays, each track striking a TOF slat provides an electronic stop at a time given by the time of flight of the particle, plus the scintillation light propagation time in the slat. The time taken by the propagation of the scintillation light in the slat is corrected for using the extrapolation of the TPC tracks as described in the previous subsection. After this correction and that for the various offsets, the time difference between the start and the stops are simply due to the times of flight of the particles striking the various slats, modified by the poor resolution of the start. The poor start resolution has the effect of shifting all time differences in a given event by a specific amount. The amount of this shift, event by event, can be determined from the TOF system and used to effectively improve the resolution of the start detector.

The correction proceeds as follows. Tracks that are consistent with being primary tracks are extrapolated to the TOF system, and a time of flight which is the stop time minus the start time is assigned to each track. One can also calculate for each track an expected time of flight using only the measured track momentum, the measured track total path length, and the assumption that the track is a pion. The difference between the measured time of flight and the actual one, assuming the particle is indeed a pion, is exactly the time shift due to the poor start resolution. If there is only one hit in the TOF system from a primary pion, the shift is measured with exactly the same resolution as the stop, or $\sim$65 ps, giving an overall resolution of the system of $\sim$92 ps. If, however, many primary tracks are measured in the TOF system in each event, the correction to the start signal is measured many times independently, and the overall resolution on the start correction improves. Given an arbitrarily large number of stops, *i.e.* an arbitrarily large number of channels of occupied TOF slats, the event by event shift in all of the time differences due to a poor electronic start signal can be corrected to an essentially arbitrary precision. The actual accuracy of the start correction possible with only one tray of 45 slats was investigated with the full simulations and the results are now described.

Central HIJING events were processed through GSTAR and the detector simulators in STAF as described above. In STAF, an random value in the range from -0.5 to 0.5 ns was sampled for each tray separately. This value was added to all of the times of flight from GSTAR+*cts* in a given tray to simulate the poor resolution of the electronic start signal from the ZDC. The goal of the simulation is the determination of the accuracy by which this random shift can be reconstructed from the tracking and TOF information in each tray and in each event. For each primary track striking a TOF slat, a "calculated" time of flight was determined using the reconstructed momentum and total path length under the assumption the particle was a pion. A histogram was formed, for each tray and for each event, of the differences between the calculated times of flight and the measured ones for slats struck only once per event by primary tracks. The bin with the most counts generally contains the pions, and the mean value of the differences between the calculated and measured times of flight in this bin defines the start correction. The open question is the bin-width used in this histogram. Larger bins will give one information to work with, improving the potential accuracy of the start correction, although larger bins also allow the possibility that kaons or protons are accidentally included in the calculation of the start correction. If this occurs, the average of the time differences is significantly skewed by the fact that the expected time of flight was calculated using an incorrect mass.

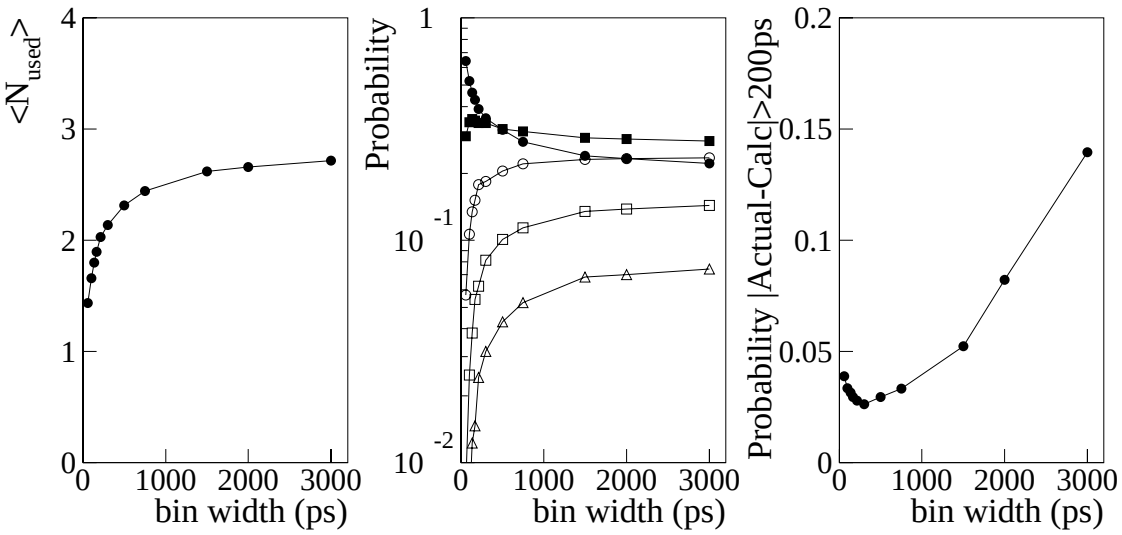

Figure 27: The dependence of various quantities related to the accuracy of reconstructing a correction to the start time as a function of the time difference bin width. For the details, see the text.

These aspects are summarized in Figure 27. The left frame shows the mean number of primary tracks used in the start correction calculation as a function of the time difference bin width. The center frame shows the probability for various numbers of primary tracks used in the start correction calculation, also as a function of the time difference bin width. The point styles correspond to the following numbers of primary tracks used in the calculation: one (solid circles), two (solid squares), three

(open circles), four (open squares), and five (open triangles). In the left and center frames of Figure 27, it is clear that as the time difference bin width increases, there are more primary tracks used in the start correction calculation. However, the right frame in Figure 27 depicts the probability that the start correction calculation breaks down. Shown is the probability that the calculated start correction exists in a non-Gaussian tail. This is due to the inclusion of a non-pion in the start correction calculation, the probability for which increases strongly with the bin width.

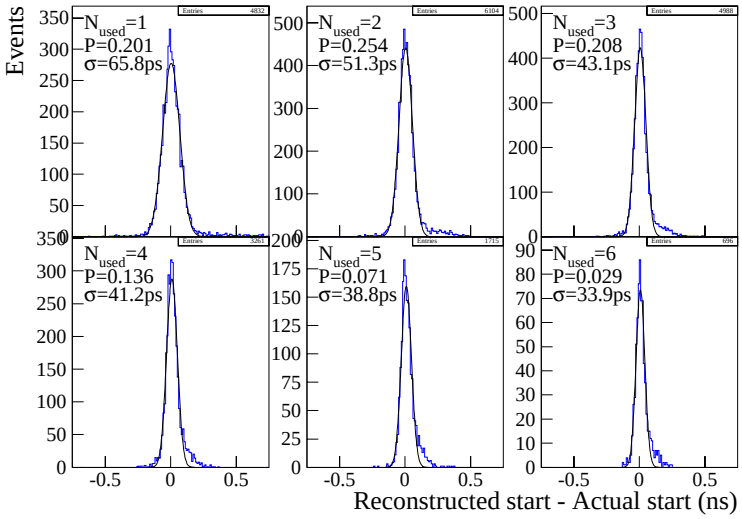

Figure 28: The difference between the reconstructed start time and the actual start time used in the full simulation of central HIJING events for the different numbers of primary tracks available for the calculation in a given event. The probability per event, and the resolution of the start time, from the calculation are labelled in each frame.

Shown in Figure 28 is the performance of the start correction when a time difference bin width of 1 ns is used. This choice is, from Figure 27, a compromise between maximizing the number of primary tracks included in the calculation, and minimizing the accidental inclusion of non-pions in the start correction calculation. Roughly 9% of the the events are not correctable no matter what the bin width, as in these events there are no primary tracks striking a singly struck TOF slat. These events are obviously excluded from subsequent TOF analyses. In 1/5 of the events, a single primary track is available for the calculation, and the resolution of the start correction is 66 ps. This is the resolution one would expect in this case, given an average slat assembly resolution of 61 ps, the 16 ps smearing from the hit position correction, and the additional smearing from the TPC momentum and path length resolutions. In $\sim$70% of the events, two or more primary tracks are available for the calculation, and the start correction then has a resolution of $\sim$50 ps or less. Approximately 4% of the events exist in tails in which the reconstructed start time is skewed by as much as a few hundred picoseconds. This can be reduced to $\sim$3% via a smaller start correction calculation bin width, at the expense of reducing the number of tracks available for the calculation. It is also possible this can be reduced farther by imposing upper lim-

its on the momenta of the TOF-incident primary tracks used in the start correction, although this cut has not yet been studied in detail.

In actual analyses, the start correction would be performed as described above and again as a function of the number of primary tracks available for the calculation. In general though, for ∼91% of the events, a sufficient start correction is possible with only one tray of TOF slats. Of these events, ∼96% have a reconstructed start time that is within $\sim 3\sigma$ of the actual value. The start resolution averaging over the number of tracks used in the calculation is 49 ps. The overall time difference resolution of the system with the present start correction performed offline is then $61 \oplus 16 \oplus 49$ ps, or 80 ps.

4.4 Peripheral Collisions

The study of hadronic spectra in Au+Au collisions versus global observables such as the number of participants or the impact parameter is an avenue to understanding how the spectra change versus the size and energy density of the reaction zone. This approach is as interesting as those which use different beam species and/or beam energies to achieve similar variations. As in central Au+Au events, the TOF system could, in principle, make significant contributions to the measurement of spectra in the large impact parameter event classes. At yet higher impact parameters, in fact well in excess of the radius of the colliding nuclei, STAR's Peripheral Physics program intends to reconstruct a number of different kinds of (low multiplicity) final states. In principle, TOF information may also be useful in this program, although these analyses have not yet been simulated with TOF information. For both, it will be by far the most common case that, if there is a hit in a TOF slat, there is only one. The sub-50 ps average correction to the poor electronic start from the ZDC that is enjoyed in central Au+Au collisions (described above) will not be possible in these events. In this section, we comment on the performance of the present system in collisions that are well less than central, where in general it will be common that there is only one hit in the TOF system per event.

Shown in Figure 29 is effectively the performance of the TOF system in this situation. Shown are the times of flight versus the track momentum without any start correction, *i.e.* by simply assuming that the resolution on the time of flight is quadrature sum of the 61 ps average slat assembly (stop) resolution and the 250 ps (start) resolution of the ZDC detector. This figure implies that, for momenta below approximately 1.2 GeV/c, pion and Kaon hypotheses can still be assigned with some certainty even under these conditions. For proton PID, direct identification is possible up to ∼2.2 GeV/c.

Clearly, peripheral events with more than one hit in the tray per event support improvements to the start correction at the levels described in the previous section. Figure 29 implies that PID via TOF in the STAR geometry is possible even in extremely low occupancy events, although the maximum momenta for direct hadronic PID are decreased significantly from the values possible with the full start correction algorithm. This allows the present system to participate in the measurement of spectra over the full range of impact parameters studied in STAR.

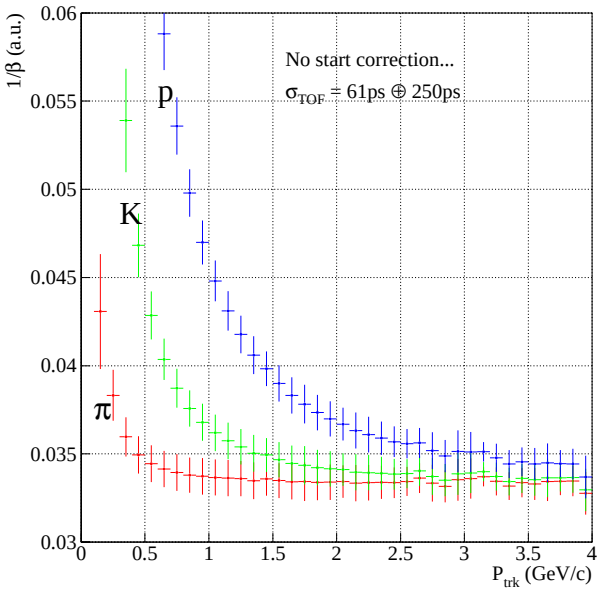

Figure 29: The inverse velocities from the TOF system versus the track momentum when the TOF resolution is the quadrature sum of the intrinsic slat resolution and the ZDC resolution. This figure simulates the performance of the TOF system in extremely low occupancy events where a start correction is generally not possible, *i.e.* in other than central Au+Au collisions.

5 Cost, Schedule, and Manpower

In this section, we summarize the cost of the present system and discuss important aspects of the schedule for the construction of the tray and its mechanical and electronic insertion into STAR. As we currently understand the STAR end game [44], there is a window in early October, 1999, during which the STAR magnet's pole tips are open and the tray can be installed.

Under this assumption, the time line for the tray construction project is presented in Figure 31. The PMTs and the scintillator slats would be ordered as soon as possible. The earlier the long ribbon cables are available, the better the possibility that they can be installed at the same time as other scheduled cable installations, so these will also be ordered early. During the two month lead time for the PMTs and slats, the electronics would be constructed. Two prototyping rounds on the CW bases, as well as the discriminator circuits, have already been completed.

A TOF electronics "system test" is scheduled for early April, 1999. In this test, $\geq$2 CW bases, $\geq$1 discriminator/CW control board, and the HDLC interface would be tested as realistically as possible. A few pieces of spare scintillator and a few of the spare CTB PMTs will be used if the final slats and PMTs are not yet available. An existing CAMAC DAQ system using LeCroy ADCs and TDCs will be used to digitize the analog and logic signals from the discriminator/CW control board to test the performance of this board and the slat assemblies. The system would be exercised using cosmics and sources, and any final optimizations to the electronics would be made.

The tray hardware with the cooling loops would be constructed during in a parallel

effort. Upon receipt of the PMTs and slats, the PMTs are burnt-in and the slat assemblies would be fabricated and graded. Following the fabrication of the final versions of the electronic, the tray is filled with the final components. A second system test is then performed with the final system before shipping. The tray will then be shipped to BNL at the end of August, 1999, and installed on the TPC with its connections.

We recognize that the primary focus of the STAR hardware efforts over the next year or so is squarely on the baseline apparatus. The present construction effort will not significantly perturb these efforts. Once constructed and shipped to BNL, the present tray need only be slid onto the appropriate rail on the TPC. The cables to be routed are small, and there is a small number of these cables. The requirements on the cooling water delivered and removed from the tray are extremely modest. The rest of the system is on the platform or beyond.

The costs of the system are summarized in Table 30. The PMT costs were obtained on 8/27/98 and depend on the dollar to yen exchange rate at the time of the actual purchase. Since this date the Yen has increased in value by ∼14% [45]. The estimate shown below is thus scaled up by 14%. Eight PMTs will be left over from the construction of the 125 CTB trays, and hence devoted to the present system, saving ∼11 k$ from the total cost.

Figure 30: The costs for the system.

Item	Source	Cost
Scintillator	Bicron	$2,964
PMTs	Hamamatsu	$52,050
CW Bases	custom	$10,100
LV power supplies	Tektronix	$1,600
Tray mechanical/cooling	custom	$1,000
Disc/CW control FEE	custom	$4,700
Ribbon cable assemblies	Amp	$4,900
HDLC interface in tray	custom	$2,400
patch panel	custom	$2,440
Crate controller	Kinetics	$9,400
Host adapter	Kinetics	$7,345
Token interface	custom	$6,050
Total		$104,949

It is assumed below that items such as the CAMAC discriminators, the CAMAC crate, and the ADCs and TDCs can be borrowed from an equipment pool. It is also assumed that 1-2 free channels in an existing Radstone board can be found and devoted to this system. If this is possible, all of the off-detector slow controls components are simply the STAR standard and already exist.

The tray construction and commissioning effort can be broken down into specific

types of tasks. Manpower is in place for each task and some efforts are already underway, although participation by any interested persons will continue to be encouraged.

I Slat Assemblies
This includes burning in the PMTs, grading PMTs, gluing PMTs to slats, masking/wrapping the slats, and grading the final assemblies. Jigs and test equipment for these tasks were developed at Rice for the CTB construction effort. The CTB construction effort will be completed in mid-January, 1999, which matches well with the schedule proposed for the present system. This equipment will therefore be devoted to the present system, and this work will be done by physicists.

II Tray Hardware
This includes the fabrication of the foam support pieces and the cooling loops, the cabling, and the various feedthroughs at the tray end. Again, these aspects are similar to those in the CTB construction, and experience exists at Rice. This work will be done by physicists.

III Electronics
These include the CW bases, the Discriminator/CW Control boards, and the HDLC interface board. Mature versions of the CW bases already exist. Two prototyping rounds of the discriminator circuit have been completed. A system test is planned for early April, 1999. This test could be performed at Rice or BNL, depending on the availability of the off-tray components of the slow controls interface. The major goal of this test is to exercise the functionality of the chain: slat $\rightarrow$ PMT $\rightarrow$ CW $\rightarrow$ Disc/CW control $\rightarrow$ CAMAC ADC/TDC (to a PC over a GPIB interface). This will require (continued) full-time participation of an engineer (N. Adams), who is at Rice.

IV Slow Controls
These include the HDLC receiver in the TOF tray and the connection to a STAR standard user interface. We assume very little development time and cost is necessary for the off-tray components, as the goal is to conform to the, now very mature, STAR standard. We will rely on the STAR Slow Controls group for some guidance here. The TOF-specific aspects of the off-tray user interface will be handled by physicists.

V Installation
This includes the insertion of the tray on a TPC rail, the routing of $\sim$6 cables (four ribbon, one HDLC bus, and the low voltage lines) from the tray end to the location of the TOF crates on the platform, and the connection of the tray cooling loop to the STAR water system. This work can be done by physicists with guidance from the STAR Integration group.

VI Digitization
This includes the NIM logic that generates TDC starts and ADC gates,

and the CAMAC hardware that performs the conversion of the analog and logic signals from the trays to pulse areas and times. We assume very little development time and cost is necessary for these aspects. The goal is to use, in an absolutely standard way, commercial units borrowed from an equipment pool or a STAR institution.

VII DAQ & Trigger Interfaces

These include the means by which the STAR trigger and clock information is placed on the backplane of the TOF CAMAC crate, and the means by which the TOF digital data is inserted into the STAR data stream. Discussions are now underway between the STAR trigger, RICH, and TOF groups to implement a common solution to the trigger clock distribution. The form at the receiver end is VME for the RICH and CAMAC for the present system, but otherwise the requirements are exactly the same. The DAQ interface is incompletely designed at present, although the basic concepts of this interface have been discussed with the DAQ group and are an acceptable starting point. We will continue to rely on guidance from the STAR DAQ and Trigger groups to complete the design of these interfaces.

VIII Software

This includes the simulation and analysis software which already exists in STAF. It also includes the programming of the CAMAC crate controller and the user interface to the slow controls system, which will be done by physicists with guidance from the STAR Slow controls and DAQ groups.

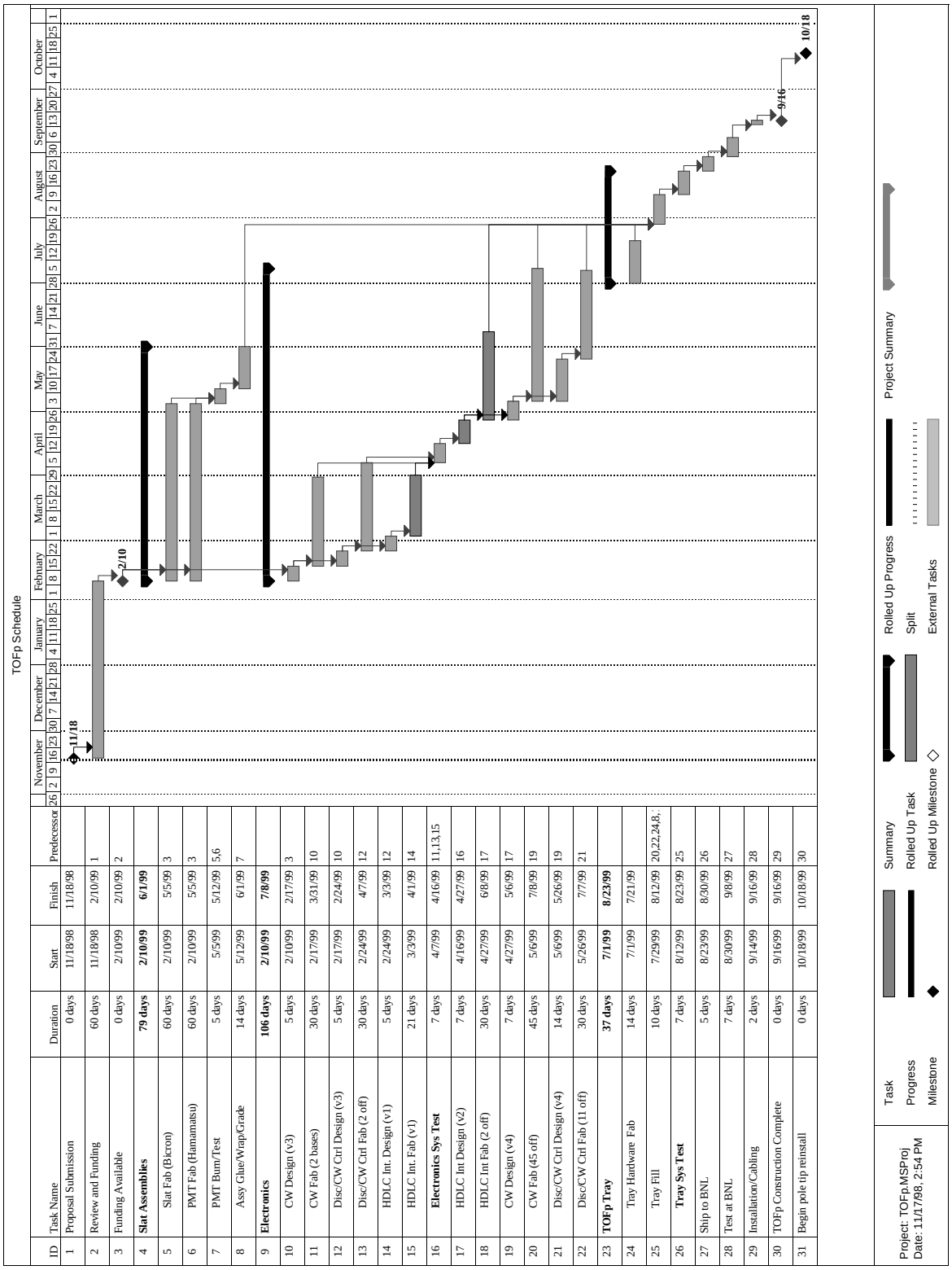

ID	Task Name	Duration	Start	Finish	Predecessor
1	Proposal Submission	0 days	11/18/98	11/18/98	
2	Review and Funding	60 days	11/18/98	2/10/99	1
3	Funding Available	0 days	2/10/99	2/10/99	2
4	**Slat Assemblies**	**79 days**	**2/10/99**	**6/1/99**	
5	Slat Fab (Bicron)	60 days	2/10/99	5/5/99	3
6	PMT Fab (Hamamatsu)	60 days	2/10/99	5/5/99	3
7	PMT Bum/Test	5 days	5/5/99	5/12/99	5,6
8	Assy Glue/Wrap/Grade	14 days	5/12/99	6/1/99	7
9	**Electronics**	**106 days**	**2/10/99**	**7/8/99**	
10	CW Design (v3)	5 days	2/10/99	2/17/99	3
11	CW Fab (2 bases)	30 days	2/17/99	3/31/99	10
12	Disc/CW Ctrl Design (v3)	5 days	2/17/99	2/24/99	10
13	Disc/CW Ctrl Fab (2 off)	30 days	2/24/99	4/7/99	12
14	HDLC Int. Design (v1)	5 days	2/24/99	3/3/99	12
15	HDLC Int. Fab (v1)	21 days	3/3/99	4/1/99	14
16	**Electronics Sys Test**	7 days	4/7/99	4/16/99	11,13,15
17	HDLC Int Design (v2)	7 days	4/16/99	4/27/99	16
18	HDLC Int Fab (2 off)	30 days	4/27/99	6/8/99	17
19	CW Design (v4)	7 days	4/27/99	5/6/99	17
20	CW Fab (45 off)	45 days	5/6/99	7/8/99	19
21	Disc/CW Ctrl Design (v4)	14 days	5/6/99	5/26/99	19
22	Disc/CW Ctrl Fab (11 off)	30 days	5/26/99	7/7/99	21
23	**TOFp Tray**	**37 days**	**7/1/99**	**8/23/99**	
24	Tray Hardware Fab	14 days	7/1/99	7/21/99	
25	Tray Fill	10 days	7/29/99	8/12/99	20,22,24,8.
26	**Tray Sys Test**	7 days	8/12/99	8/23/99	25
27	Ship to BNL	5 days	8/23/99	8/30/99	26
28	Test at BNL	7 days	8/30/99	9/8/99	27
29	Installation/Cabling	2 days	9/14/99	9/16/99	28
30	TOFp Construction Complete	0 days	9/16/99	9/16/99	29
31	Begin pole tip reinstall	0 days	10/18/99	10/18/99	30

Figure 31: The schedule for the tray construction. The tasks are labelled by the number of working days to complete, of which there are five per (40 hr) week.

6 Cost vs. Physics Reach in Alternative Designs

We have proposed a system for TOF measurements in STAR that costs approximately 100 k$. The system described in section 3 is capable for all of the analysis and physics goals outlined in section 2. We believe the ratio of physics impact to cost is maximized in the proposed design. Nonetheless, we describe in this section a few alternative designs. These alternatives would result in some savings in labor and/or equipment costs, but the physics reach of the system may also be decreased. For each alternative, our views on the pro's and con's are listed to facilitate informed discussions on these designs.

One of the design decisions described in section 3 has an alternative, but this choice does not significantly impact the physics reach of the system. This is the decision to use low voltage connections and CW bases to provide the high voltage to the PMTs, as opposed to high voltage connections and resistive bases. The use of HV and resistive bases would have the following advantages. The HDLC interface would be simplified resulting in a modest cost savings there. High quality linear bases from Hamamatsu cost approximately $175 each, which is a savings of $25 per base, or about $1,250 total compared to the CW bases. The disadvantages are the following. The power generated inside the tray would increase significantly, which would place more stringent requirements on the cooling water needed to maintain acceptable temperature levels inside the tray. A 16 stage linear Hamamatsu base has a total resistance of $\sim$6 MΩ, which at 2500 V would generate a power of $\sim$1 W per base. This is a factor of three larger than that generated by a CW base. A second LeCroy 1440 mainframe HV unit would be needed on the platform, as the existing unit for the CTB and ZDC HV is full. The main complaint with a HV-based system however concerns the cabling and feedthroughs. Instead of routing $<$5 low voltage cables from the platform to the tray, it would be necessary to run 45 high voltage cables. There is simply no room at the tray end to accommodate 45 SHV connectors.

One could imagine grading the PMTs so that groups of PMTs with similar gains are powered by a single HV cable, which would reduce the number of HV cables and the number of feedthroughs needed. This is however not an attractive approach if one wants this system to perform over periods of years. The individual PMTs may age over long time scales differently, so PMTs with reasonably matched gains on Day 1 will slowly become more poorly matched. One would not expect the relative gains to be as well matched should it be decided to run the TOF PMTs at some other overall gain. Most importantly though, it is crucial in PMT-based TOF systems to insure the pulse *heights, not areas,* are similar and can be kept that way indefinitely. As the shapes in time of the PMT signals are similar if the pulse heights are well matched, the rise time for each channel at voltages near the discriminator threshold is controllable given precise control of the PMT gain. The timing performance via the slewing correction depends importantly on the relationships between the rise time, the pulse height, and the discriminator level. If it is not possible to control the gain of each PMT separately, there is the possibility that any long term aging in the tubes will lead to wildly different magnitudes of the slewing corrections and hence different absolute time resolutions for each slat.

Now described are two alternative designs that lead both to decreases in the cost and the physics reach of the system. These are characterized by a reduction in the number of slat assemblies in the tray. In both, $\geq$6 slats would still front the RICH detector, so all of the algorithmic cross checks between the TPC, TOF, and RICH PID approaches are still possible. In neither alternative are there fewer slat assemblies simply because the slats are made larger. Because of the already high occupancy in central Au+Au collisions (*cf.* section 4.1), it is not possible for physics reasons to consider larger slats.

One could replace only the low-rapidity CTB slat in a tray with TOF slats. This would reduce the overall cost by $\sim$35 k\$ for PMTs and $\sim$10 k\$ for electronics. The penalties are the following. The mechanical aspects of the interior of the "hybrid" tray would be relatively complicated, but not excessively so. The total solid angle subtended by TOF counters would drop by a factor of two. The resolution of the start correction would suffer significantly, as a factor of two fewer primary tracks would be available the calculate the correction. From a physics standpoint, reasonable measurements of transverse momentum spectra for identified hadrons would then take a factor of two longer. Finally, the reduction in the pseudorapidity coverage reduces the phase space coverage, which reduces the sensitivity of, *e.g.*, net proton analyses. If the largest pseudorapidity with TOF coverage is 0.95(0.5), the largest rapidity with TOF coverage is 0.51(0.31) for 0.8 GeV/c protons, and 0.88(0.47) for 3 GeV/c protons.

The other alternative is to remove rows in azimuth. In the proposed design (*cf.* figure 14), there are nine groups of slats in rapidity, and in each of these, there are five rows of slats in azimuth. Removing, *e.g.*, the second and fourth rows in azimuth would reduce the number of slat assembles from 45 to 27, again saving $\sim$35 k\$ for PMTs and $\sim$10 k\$ for electronics. The full rapidity coverage of the proposed design is retained. However, as in the other alternative design, the geometrical acceptance decreases by a factor of two. This again compromises the quality of the necessary start correction, and requires event samples that are twice as large to make similarly certain measurements of momentum spectra. Gaps in the coverage of scintillators on the outer area of the TPC cylinder would exist, which bears on the use of the CTB and TOF slats in the trigger. Finally, the utility of the system for interferometric analyses are decreased, as the acceptance of the system for low relative momentum pairs of TOF-identified particles is decreased.

In both alternatives, the reduced coverage results in a degradation of the time resolution of the system by reducing the accuracy of the start correction. The reduced coverage furthermore implies that important physics analyses are compromised statistically. Studies of small EbyE samples, of high P_T particles, and of interferometry in three or more dimensions will suffer. We thus conclude that in the overall context of STAR's unique role in the RHIC physics program, any technically feasible scenario for reducing the cost of the proposed TOF patch results in a serious and disproportionate erosion of the enhanced physics capabilities.

References

[1] http://bonner-mac8.rice.edu/~WJLlope/-STAR/-TOF/TOFprop.html.

[2] http://bonner-mac8.rice.edu/~WJLlope/-STAR/-TOF/TOFpatch.html.

[3] STAR Notes 36 (1992), 49 (1992), 50 (1992), 52 (1992), 207 (1995), 208 (1995), 209 (1995), 211 (1995), 267 (1996), and 326 (1998).

[4] http://www.er.doe.gov/production/henp/nsac/nsac.html

[5] B. Lasiuk, STAR Note 312 (1997).

[6] "Proposal for a Ring Imaging Čerenkov Detector in STAR", Yale University (1998), available from http://star.physics.yale.edu/PapersAndNotes.html

[7] X.N. Wang, Phys. Rep. **280**, 287 (1997).

[8] H. Sorge, Phys. Rev. C **52**, 3291 (1995).

[9] K. Werner, Phys. Rep. **232**, 87 (1995).

[10] R. Anishety *et al.*, Phys. Rev. D **22**, 2793 (1980);
W. Busza *et al.*, Phys. Lett. B **139**, 235 (1984);
S. Date *et al.*, Phys. Rev. D **32**, 619 (1985).

[11] W.M. Geist, Phys. Lett B **211**, 233 (1988).

[12] X.N. Wang *et al.*, Phys. Rev Lett. **68**, 1480 (1992).

[13] A. Dumitru and D.H. Rischke, Preprint nucl-th/9806003.

[14] S. Uddin and C.P. Singh, Phys. Lett. **B278**, 357 (1992).

[15] A. Dumitru, private communication.

[16] W.J. Llope, Plenary talk, STAR Collaboration Meeting, January, 1998.

[17] J. Cramer, private communication.

[18] Report from the STAR Task Force on Computing Requirements, P. Jacobs *et al.*, available from http://www.rhic.bnl.gov/STAR/html/comp_l/ofl/reqmts9708.

[19] S. Suzuki et al., IEEE Trans. on Nucl. Sci. **33**, No. 1, 377, (1986); G. Finset et al., Nucl. Inst. and Methods **A290**, 450 (1990).

[20] A. Ahmad *et al.*, Nucl. Inst. and Methods, **A330**, 416 (1993).

[21] Bicron Corporation, 12345 Kinsman Rd., Newbury, OH.

[22] R.E. Bell, Nucl. Inst. and Methods, **42**, 211 (1996).

[23] A. Hauger *et al.*, STAR Note 86.

[24] S. Cova *et al.*, Nucl. Inst. and Methods **A253**, 482 (1987);
N.S. Nightingale, Exp. Astronomy **1**, 6 (1991);
H. Fenker, SSC Preprint SSCL-120 (1992).

[25] H. Fenker *et al.*, SSC Preprint SSCL-458 (1993);
R.G.W. Brown *et al.*, App. Optics **26**, 2383 (1987),
S. Cova *et al.*, IEEE Trans. Nucl. Sci. **29**, 599 (1982).

[26] http://PesTOF.GSI.DE/source/PesTOF_home.html.

[27] A. Ahmad *et al.*, Nucl. Inst. and Methods, **A400**, 149 (1997).

[28] Oaks Precision Manufacturing, Inc., 3550 Breen Drive, Houston, TX.

[29] General Plastics Manufacturing Company, P.O. Box 9097, Tacoma, WA.

[30] T. Abbott *et al.*, Nucl. Inst. and Methods **A290**, 41 (1990).

[31] R. LaCasse *et al.*, Nucl. Inst. and Methods **A408**, 408 (1998).

[32] W.J. Llope *et al.*, http://bonner-mac8.rice.edu/~E896/default.html

[33] http://products.analog.com/products/info.asp?product=AD96687, and
http://www.analog.com/pdf/96685_87.pdf.

[34] T. Kobayashi and T. Sugitate, Nucl. Inst. and Methods, **A287**, 389 (1990).

[35] Amphenol part no. 121-3001-025; Spectra-Strip Cable Products, 720 Sherman Avenue, Hamden, CT.

[36] http://www.tek.com/Measurement/Products/catalog/ps280/index.html.

[37] http://209.1.238.250/arpdf/1469.pdf, from
http://www.maxim-ic.com/Products.htm.

[38] http://209.1.238.250/arpdf/1591.pdf, from
http://www.maxim-ic.com/Products.htm.

[39] R. Bellwied, private communication.

[40] H. Strobele, Plenary talk, STAR Collaboration Meeting, July 1998.

[41] R. Sumner and G. Blanar, http://www.lecroy.com/lrs/PUBS/P43/P43.htm.

[42] G. Varner *et al.*, http://www.phys.hawaii.edu/ bellemgr/
G. Varner *et al.*, http://www.lecroy.com/lrs/pubs/p52/p52.htm.

[43] M. Levine, private communications.

[44] J. Harris, private communication.

[45] http://www.barchart.com/cme/cmejy.htm.